

NRL REPORT 3814

DIELECTRIC-GUIDE ANTENNAS FOR AIRCRAFT

F. E. Boyd and D. H. Russell

October 19, 1951

APPROVED FOR PUBLIC
RELEASE - DISTRIBUTION
UNLIMITED

Approved by:

F. M. Gager, Head, Special Research Branch
R. M. Page, Superintendent, Radio Division III



NAVAL RESEARCH LABORATORY

CAPTAIN F. R. FURTH, USN, DIRECTOR
WASHINGTON, D.C.

DISTRIBUTION

OpNav		
Attn: Op-42		2
ONR		
Attn: Code 470		1
Attn: Mr. H. Harrison, Code 427		1
BuAer		
Attn: Mr. E. P. McDowell, Code EL-411		1
Attn: Mr. E. L. Rogers, Code EL-433		1
Attn: Mr. Gordon Clark, AR-66		1
BuOrd		
Attn: Mr. A. D. Bartelt, Code Re4f		1
BuShips		
Attn: Mr. Alfred W. Andrews, Code 833		1
CO & Dir., USNEL		2
Attn: Dr. T. J. Keary		1
Attn: Dr. F. R. Abbott		1
CDR, USNOTS		1
Attn: Reports Unit		2
Supt., USNPGS		1
Dir., USNUSL		
Attn: Mr. C. M. Dunn		1
CDR, USNPG, Dahlgren		1
CDR, NADC		
Attn: Dr. H. Krutter		1
Attn: Mr. E. Steel		1
Attn: Mr. E. R. Schlieben		1
CDR, NATC, Patuxent River, Md.		
Attn: Electronics Test, Antenna Section		1
Wright-Patterson AFB		
Attn: BAU-CADO		1
Attn: CADO-E1		2
Attn: Mr. T. J. Gibbons, MCREEO		1
Attn: Ch., Eng. Div., MCREEO-2		1

OCSigO	
Attn: Ch. Eng. and Tech. Div., SIGTM-S	1
Attn: Mr. J. J. Kelleher	1
Attn: Mr. A. R. Beach	1
CG, SCEL	
Attn: SCEL Liaison Office	3
Dir., ESL	
Attn: Mr. O. C. Woodyard	1
Attn: Mr. Leonard Moore	1
Chief of Staff, USAF	
Attn: Mr. Joseph Weichbrod	1
CO, 3151st Electronics Group, Griffiss AFB Rome, New York	
Attn: ENR	1
CO, Air Force Cambridge Res. Labs.	
Attn: Dr. R. C. Spencer	1
Attn: Mr. R. M. Barrett	1
Attn: ERRS	1
Dir., NBS, Central Radio Propagation Laboratory	
Attn: Dr. Harold Lyons	1
Attn: Dr. Harold Goldberg	1
Attn: Dr. A. G. McNish	1
RDB	
Attn: Information Requirements Branch	2
Attn: Navy Secretary	1
Attn: Mr. M. Barry Carlton, Committee on Electronics	1
Attn: Panel on Antennas and Propagation	25
Naval Res. Sec., Science Div., Library of Congress	
Attn: Mr. J. H. Heald	2

CONTENTS

Abstract	vi
Problem Status	vi
Authorization	vi
INTRODUCTION	1
Classification of Dielectric-Guide Antennas	1
Symbols and Terms	1
THEORETICAL DATA	4
Radiation Considerations	4
Impedance Considerations	8
SCOPE OF THE EXPERIMENTAL WORK	9
Antennas for Toroidal Beams	9
End-Fire Radiators	10
GEOMETRIC PARAMETER EFFECTS	12
Aperture	13
Length	14
Tapers	14
DESIGN PRINCIPLES	17
Design Frequency	19
Dielectric Materials	19
Feed Design	22
Array Design	23
Gain Considerations	23
Beamwidth Considerations	24
Sidelobe Considerations	26
Aerodynamic Factors	26
Reinforcement	28
DESIGN PROCEDURE	29

FREE-SPACE MEASUREMENTS	31
Uniform Rods	31
Uniform-Taper Rods	31
Two-Taper Rods	32
Three-Taper Rods	32
Asymmetrical Rods	35
Tubes and Stepped Rods	35
Arrays	35
Impedance	35
Power Capacity	38
Bandwidth	38
Polarization	38
FUSELAGE PROXIMITY MEASUREMENTS	38
Standing-Wave Ratio	39
Proximity Limitation	39
Pattern Tests	39
Effects of Mounting Distance upon Patterns, $\phi_A = 0$	41
Effects of Antenna Angle upon Patterns, $D = 6.3\lambda_0$	41
Tracking Tests	43
Tracking Records	44
CONCLUSIONS	45
RECOMMENDATIONS	45
REFERENCES	47
APPENDIX - Measurement Techniques	49

ABSTRACT

An investigation was made of dielectric-guide antennas suitable for airborne radar applications. The study was directed toward streamlined and recessed types having compact design, minimum weight, and low minor lobe radiation. Of the many forms investigated, the tapered polystyrene rod (polyrod) is the most practicable. Highly directive polyrods weigh 6 ounces and are 9 inches long at 10,000 Mc, but lengthen in direct proportion to wavelength. Sidelobe reduction to at least 17 db is possible by properly dimensioning the rod; minimum practical beamwidth for a single rod is 21° , and maximum gain is 18 db, obtained with a polyrod 7.5 wavelengths long. These characteristics are not mutually obtainable, but excellent compromises can be made. Arrays may be used to obtain narrower beamwidths and higher gains. Several methods have been found of strengthening the polyrod, which should allow its use in wind streams of order 580 knots at 20,000 feet altitude. Radiation measurements made on a specially designed series of polyrods are included to facilitate the design and development of end-fire rods and broadside arrays for particular applications. Radiation effects of mounting the polyrod near aircraft fuselages were also recorded.

PROBLEM STATUS

This is a final report on the problem. If not otherwise notified by the Bureau, the problem will be considered closed one month from the mailing date of this report.

AUTHORIZATION

NRL Problem R09-34D,
NL 490-124

Manuscript submitted for publication: May 21, 1951

DIELECTRIC-GUIDE ANTENNAS FOR AIRCRAFT

INTRODUCTION

Airborne dielectric-guide antennas are technically usable throughout the radio frequency spectrum. They are practicable throughout the microwave region corresponding to about one-half to thirty centimeter wavelengths. Within this range they indicate wide application to aircraft radar, since they provide either end-fire or broadside directivity in very compact form, in conjunction with a limited amount of radiation-pattern control.

The theory of electromagnetic wave propagation along dielectric materials has been treated by many authors.* In general, the theoretical state of the art is such that the calculated radiation patterns of most any antenna configuration do not agree with measurements, and especially is this true with the sidelobe configuration. In consequence, an experimental method of establishing fact was employed.

Dielectric-guide antennas, as the term is used in this report, includes any configuration where directivity is obtained mainly by virtue of linear length. This definition includes dielectric horn, solid-rod and hollow-tube type antennas where the transverse dimensions are on the order of a vacuum wavelength or less and the longitudinal dimension is several times as great. Dielectric-lens antennas and short, thick tubes are therefore excluded from this study.

Experimental work with tapered rods at 9375 Mc was undertaken to expedite applicational optimum design throughout a large range of frequencies. Short dielectric tubes, which are attractive from the standpoint of high-strength requirements, were also studied, but sufficient work was not done to arrive at their optimum design. The performance of the polyrod for arrays was investigated, as well as the effects of simulated flat aircraft fuselages near the polyrod.

Classification of Dielectric-Guide Antennas

Dielectric-guide antennas may be subdivided into twelve basic forms of which various combinations and modifications are possible. Figure 1 shows longitudinal-section views (in a plane at right angles to the aperture). Feed details are not shown, but stub, dipole, or metallic guide means will suffice.

Symbols and Terms

Symbols and terms used throughout this study are listed and defined in Table 1.

* Listed in References

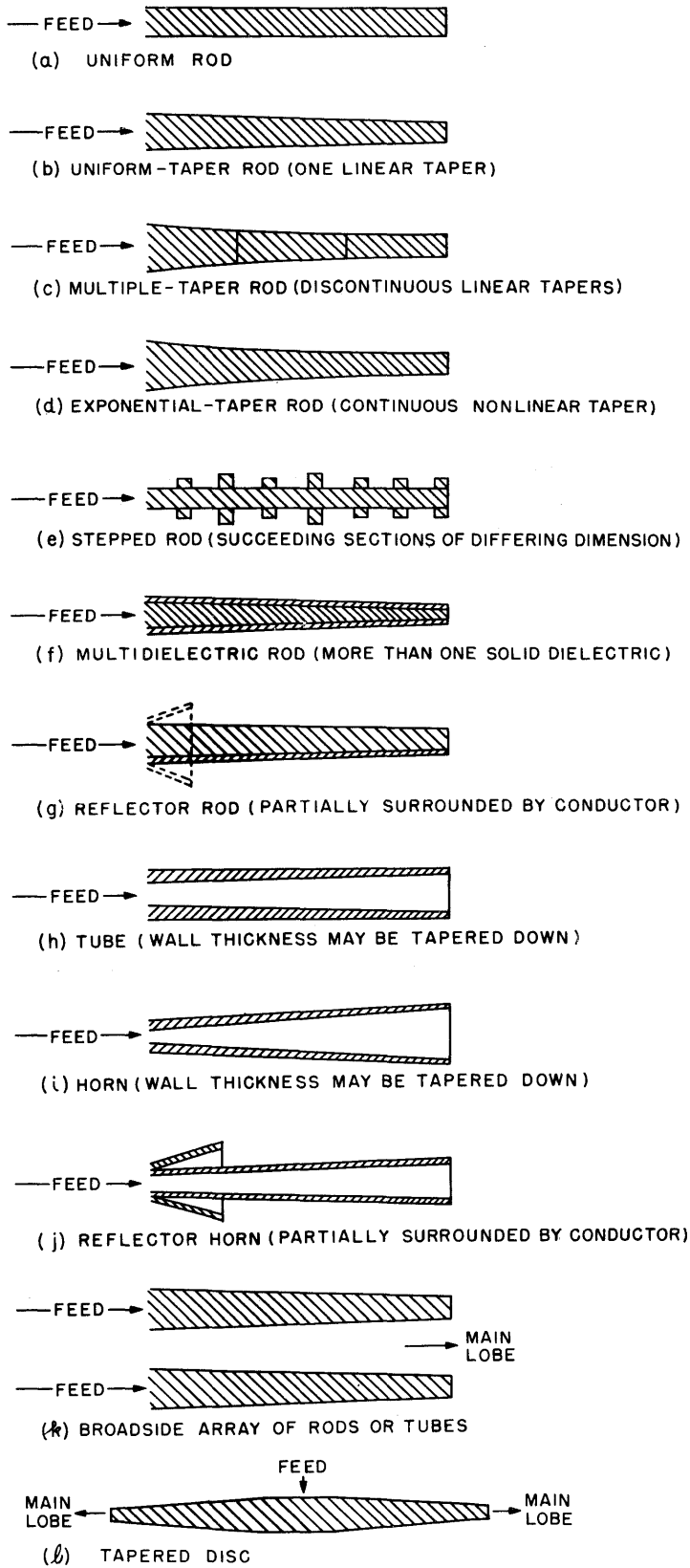


Figure 1 - Basic forms of dielectric-guide radiators

TABLE 1
Symbols and Terms

Symbol	Term	Meaning
G	Absolute gain	Main-beam gain relative to isotropic radiator (affected by antenna losses)
BW	Half-power beamwidth	Angular width of main beam at 3 db points
SL	Sidelobe depth	Depth of maximum sidelobe below main beam
α	Dissipation	Power loss
P	Directivity	Absolute gain, lossless antenna
e	Dielectric constant	Relative real value (17)
$e \tan \delta$	Loss factor	Relative value (17)
Subscript o		Refers to free-space value
Subscript r		Refers to value in radiator
Subscript g		Refers to value in metal guide
Subscript f		Refers to value at feed end of radiator
Subscript 1		Refers to dimensions at feed end of radiator
Subscript 2		Refers to dimensions at free end (termination) of radiator
λ	Wavelength	Wavelength in any medium
λ_c	Cutoff wavelength	Wavelength for dominant mode in metal guide
v	Phase velocity	Phase velocity in any medium
c	Velocity	Phase velocity in free space
Z	Wave impedance	Ratio of the electric to the magnetic field strength each normal to the direction of propagation
d	Diameter	Transverse dimension
w	Width	Transverse dimension
A	Area	Transverse section area
L	Radiator length	Length of radiator portion of antenna
l	Taper length	Length of tapered portion of radiator
l'	Wrapped length	Length of tapered wrapping over radiator
ψ	Taper angle	Angle included between profiles of any tapered guide
A_2/A_1	Taper factor	Taper defined as area ratio
D	Distance	Linear measurement between antenna and ground plane
s	Distance	Spacing between adjacent elements in an array
F	Fiber stress	Mechanical stress in psi
S	Length	Length of fuselage

THEORETICAL DATA

The theory of electromagnetic radiation along a dielectric medium of finite cross-dimension and the experimental verification of such a phenomenon have been treated by previous investigators. A review of the mathematical analyses indicates that no rigorous solution has been accomplished save for the abstract case of a uniform infinite rod. The various theories extant for the design of dielectric radiators have not been found to be in good agreement with the performance of tapered radiators, especially regarding sidelobes. A rigorous formulation of the radiation characteristics has not been established as a function of the governing parameters.

Carson, Mead, and Schelkunoff (1), and Wegener (19) and others have contributed to uniform infinite rod theory, yielding data which may be applied only qualitatively to tapered rods of finite length. Mallach (10), Mueller and Tyrrell (13) and others have published empirical solutions which purportedly prophesy the characteristics of certain rods from an engineering viewpoint—they do not yield exact agreement with results obtained in this study, however, even for simply tapered rods. Further analysis is under way at several establishments (12).

The limited theoretical aspects of the subject herein considered are most readily divided into two phases, not completely distinct from each other: first, a review and experimental verification of the theoretical data applicable to radiation from a dielectric configuration, without thought of the impedance details; second, considerations of feed impedance as well as impedance distribution along the radiator. Clarification of the part played by the impedance discontinuity along the length of the rod, as seen by the progressively radiating wave, should aid further efforts in formulating the radiation theory of tapered rods.

Radiation Considerations

The dielectric rod radiator, excited by a probe, dipole, or metallic waveguide operating in the dominant mode, propagates a hybrid dominant wave (Figure 2) such as that shown by Wegener (19). The wave is axially asymmetric and contains electric and magnetic components in the longitudinal direction, as well as in the transverse dimension. The cross section corresponds more closely to that of an H-wave than an E, and the phase changes once around the periphery, for which reasons Wegener designated it as the HE_{10} wave. In detail, the wave corresponds closely with the H_{10} mode of a square waveguide feed, or the H_{11} mode of a circular feed. The correspondence is not perfect because a portion of the energy is external to the dielectric, the longitudinal conduction currents of the metallic feed are replaced by longitudinal displacement currents about the dielectric, and progressive radiation ensues along the rod. The electric field components in a cross-sectional surface have the same phase and a preferential direction. Since the resultant of the electric lines remains parallel to that of the feed, and because of the equiphase field cross section within the rod, good feed-matching and directivity can be obtained.

Control of the HE_{10} phase and energy distribution, which determines the radiation pattern from a rod radiator, is effected by choice of the dielectric material, aperture area at the feed-junction, and radiator length and taper. Phase and amplitude of the radiation components are not independently controllable by parametric variation, so that pattern control is limited.

The HE_{10} mode is guided for all finite wavelengths, so that the cutoff frequency is zero. The next higher modes cannot be guided by narrow rods. For example, Wegener's

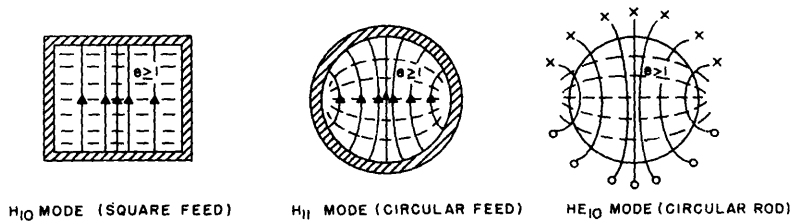


Figure 2 - Aperture field configurations for the dominant feed and radiator modes—E-lines solid, H-lines dashed

solutions, applied to polystyrene, indicate that the higher modes are cut off for rod diameters less than $0.62 \lambda_0$. For any value of dielectric constant, HE_{10} single-mode propagation theoretically can be obtained concurrently with apertures yielding maximum directivity.

The amplitude of the radiation component from a uniform rod at a given cross section is dependent among other factors upon the section area of the rod at that point. The theoretical ratio of external to internal energy as a function of the ratio of the cylindrical rod diameter to the free-space wavelength is shown in Figure 3 for dielectric constants 2.55 and 10. When tapering is employed, general theory would dictate that the external energy intensity would decrease with increasing effective dielectric constant, whereas the same reasoning makes the external energy gradually increase along tapered rods in the direction of the smaller cross sections. A single universal curve (a plot of the energy ratio against $d\sqrt{\epsilon}/\lambda_0$ and applying to all values of dielectric constant) does not physically exist since the retaining effect (discontinuity) of the dielectric interface increases with the dielectric constant. Thereby, another family of curves is evident which are quasi-superimposed. The data employed to compose Figure 3 is due to Mueller and Tyrrell (13).

The internal velocity to free-space velocity ratio as a function of the ratio of the rod diameter to the free-space wavelength is shown in Figure 4. Theoretically the wavelength within the rod asymptotically approaches the intrinsic wavelength of the dielectric for a certain value of rod diameter, d , which is approximated by a single expression involving dielectric constant, ϵ , and wavelength, λ_0 , $d = k\lambda_0/\sqrt{\epsilon-1}$. In addition it may be seen that the rod wavelength (or phase velocity) increases along the tapered rod in the direction of smallest cross section, closely approaching the free-space value at a finite diameter approximated by the same type of expression as above.

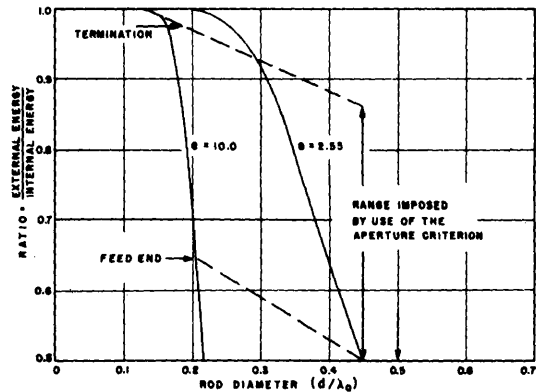


Figure 3 - HE_{10} energy distribution vs. aperture

Figure 4 was computed using Wegener's expressions and Lindner's graphical solution and to some extent it is verified by the present investigation and by other writers (13). In addition, this figure provides a design criterion in the form of two boundary curves, which at any specified frequency and dielectric constant determines the terminal cross sections of a slowly tapered uniform-taper rod possessing a certain type of phase characteristic. That is, as the rod aperture decreases along the axis, the rod wavelength increases at an ever-decreasing rate.

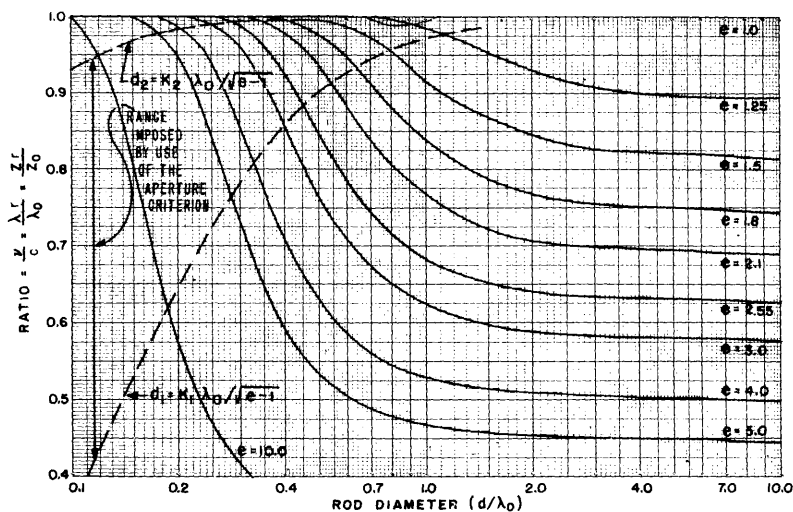


Figure 4 - HE_{10} phase velocity vs. aperture dimension for uniform dielectric rods (19)

It will be seen that a very important factor in the performance of dielectric-guide antennas is the cross-sectional area of the dielectric and the manner in which it varies along the rod. This cross-sectional area will be referred to as aperture area. The point where radiation begins is termed the feed aperture area (A_1) while the other extreme of the dielectric-guide antenna is called the terminating (free) aperture area (A_2).

Mallach stated that uniformly tapered rods should be dimensioned so that the aperture area varies approximately from 0.25 to 0.10 of $\lambda_0^2 / (\epsilon - 1)$ from the feed end to the terminating (free) end of the rod. This will be referred to as the aperture criterion. In addition, Mallach stated that the rod wavelength, λ_r ,* should be no less than $0.8\lambda_0$, a phase-velocity criterion. Figure 4 shows that these criteria are not simultaneously obtainable for dielectric constants greater than 4. According to the available reports, Mallach successfully used these criteria in designing uniformly tapered rods for dielectric constants at least up to 64. The phase-velocity criterion was not checked in this investigation as ceramics and plastics of dielectric constant greater than 4 were not used.

The aperture criterion approximates maximum directivity by maintaining a favorable axial distribution of external energy and phase velocity of the guided wave over a large range of dielectric constants (at least 2.5 to 4). The writers have experimentally verified the merit of this criterion for long uniform-taper polystyrene rods. Sidelobes of long rods are poorly suppressed, but it is possible to further reduce the sidelobes without appreciably affecting the directivity by using a multiple-taper design, consisting of additional taper sections followed by a zero-taper extension. It will be shown that a larger input aperture (than that given by the aperture criterion) should be used for optimum results with very rapidly tapered rods.

According to the aperture criterion the thickness and weight of dielectric rods may be decreased by use of higher dielectric constants. However, the length required for a given

*Analogous to guide wavelength, i.e., phase wavelength inside the rod

directivity is not affected by change of dielectric constant; i.e., the rod thickness must also be changed in such a manner that the effective rod wavelength and the radiator length for optimum radiation remain unchanged. Although Mallach used materials of very high dielectric constant, their application to airborne equipments is quite restricted, since such presently available materials result in narrow rods of poor strength. In addition, dielectric losses increase with dielectric constant, resulting in somewhat lower gain. A lower practical limit for the dielectric constant is established due to the inability of the rod to sufficiently retard the guided wave even with extremely large apertures.

Measurements show that increasing the radiator length L/λ_0 past a certain critical value reduces the gain. Following simple, linear, end-fire array theory, the progressive radiation components must combine within 180 degrees phase-shift along the rod, in order to contribute constructively to end-fire directivity. Each contribution travels a different distance before liberation from guided form, and consequently, experiences a different phase-shift. Assuming all the energy is radiated before the termination, the approximate critical length is obtained as follows, where $B_r = 2\pi/\lambda_r$ is the effective rod phase-constant:

$$B_r L - B_0 L = \pi,$$

$$\frac{L}{\lambda_r} - \frac{L}{\lambda_0} = \frac{1}{2}, \text{ and}$$

$$\frac{L}{\lambda_0} = \frac{1}{2(\lambda_0/\lambda_r - 1)}$$

In order to verify this and the data of Figure 4, at least for one point, the rod wavelength was measured along a uniform styramic rod ($e = 2.6$). Radiator wavelength, λ_r , measured $0.91 \lambda_0$ whereas Figure 4 yields a theoretical value of $0.92 \lambda_0$ for the diameter used. Though this discrepancy is small, it causes an appreciable error in the equation for critical length, which calculates to be $5.1 \lambda_0$ in the first case, and $5.7 \lambda_0$ in the second.

Figure 5 shows the variation of main-lobe gain with radiator length measured with this same rod. A slight oscillation may be noticed superimposed upon the basic curve, which apparently is caused by radiation through the end face of the rod and partially obscures the desired phenomenon. The average critical length measured over a range of $15.1 \lambda_0$ is seen to be $5.0 \lambda_0$, which closely checks the $5.1 \lambda_0$ value obtained for this rod.

Qualitatively, the same results are undoubtedly obtained with the tapered rods, but an experimental determination of critical length requires rods of impractical length—longer than those constructed. Figure 5 also illustrates the gain variation with length obtained with a series of uniform-taper rods. The curve is smooth, indicating very little radiation through the end face of these rods. In these cases B_r is a function of position (or distance) along the rods. The complete theory of the

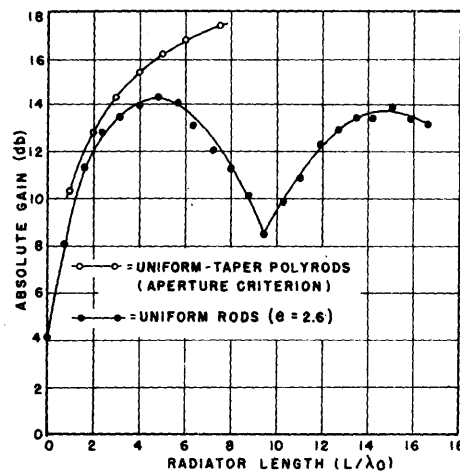


Figure 5 - Gain vs. radiator length

effective rod wavelength of tapered dielectric rods is somewhat in doubt and not available from the present theory. A rough measurement by means of a small travelling dipole yielded $\lambda_r = 0.97\lambda_0$ for uniform-taper rods complying with the aperture criterion, indicating a critical radiator length of $16\lambda_0$, and a maximum directivity of 18-19 db. Such a length is impracticable for general airborne application even with the large apertures which are afforded by the lowest dielectric constants. The increase of gain is relatively slow above $L = 7.5\lambda_0$, for which 17.4 db was obtained with uniform tapering.

The use of odd multiples of the critical length as an end-fire rod array is impracticable because of rapid field depletion, as well as rod shielding and mechanical difficulties. However, broadside arrays are quite practical because of the small apertures involved, and the induction and radiation coupling between rod elements is low.

Impedance Considerations

Adopting Schelkunoff's definition of wave impedance as the ratio of the electric to the magnetic field strength normal to the direction of propagation, Wegener has

shown that for uniform dielectric cylinders the impedance of the HE_{10} wave is, to a good approximation, $Z_r = Z_0\lambda_r/\lambda_0$, where $Z_0 = 377$ ohms. The same form $Z_g = Z_0\lambda_g/\lambda_0$, applies to the H_{10} and H_{11} waves in the square and circular feed guides, respectively.

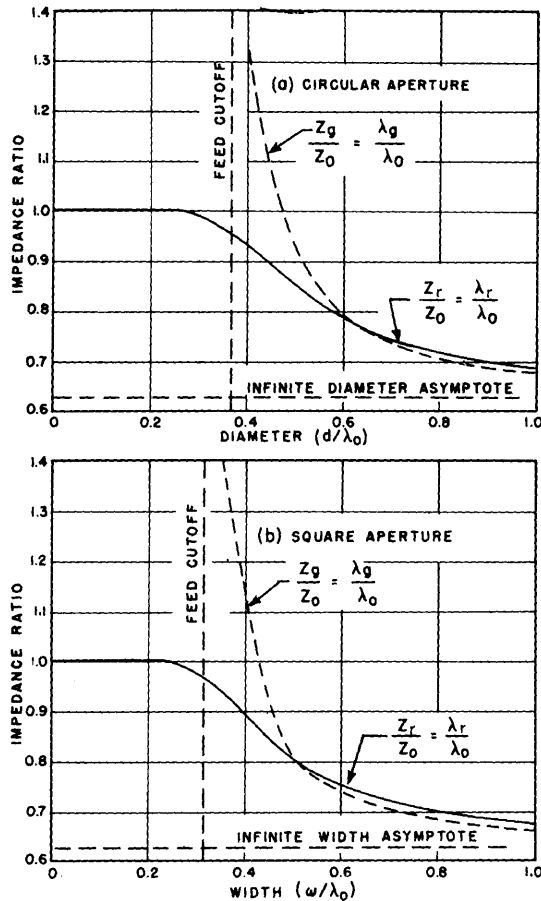


Figure 6 - Theoretical feed and radiator impedances vs. aperture dimension for uniform polyrods of circular and square apertures

Figure 6 shows impedances normalized to Z_0 for circular and square aperture polyrods. Considering $d = 0.45\lambda_0$ (or $v = 0.40\lambda_0$), which is favorable to radiation from uniform-taper rods, we note that Z_g/Z_r is on the order of 1.25 for equal rod and feed apertures. This theoretical vswr approximately checks measurements of the corresponding rods. Enlarging the feeds corresponds to approaching higher mode cutoff in the feeds; however, enlargement of the radiator above the feed dimensions causes little change in the rod impedance or the mismatch.

The impedance discontinuity at the feed junction of uniform rods may be expressed by the voltage reflection coefficient $\Gamma_1 = (Z_r - Z_g)/(Z_r + Z_g)$, assuming that the shunt susceptance introduced by the discontinuous conducting surfaces is negligible. Measurements of polystyrene rods in an attempt to determine the degree of this discontinuity showed them to be practically resistive, indicating the field along the initial portion of the dielectric to be substantially that within the feed except for the slight change in resistance. The theoretical and measured magnitude of the voltage reflection is shown

in Figure 7 plotted versus aperture for the circular and square types with the feed and rod dimensions equal. The theoretical Γ_1 applies to tapered rods if it is assumed that Z_R is not a function of taper. The experimental agreement is believed good, considering the theoretical approximations and the effect of slight internal feed reflections. Qualitatively the impedance match is seen to improve with increasing aperture, and is good in the range of the most directive diameters and widths.

The impedance discontinuity at any distance along the uniform polyrod expressed theoretically by $\Gamma_2 = (Z_0 + Z_R) / (Z_0 - Z_R)$, is plotted in Figure 8 versus diameter. Again neglecting the part that taper might play in the expression for Z_R , this may be considered to apply to tapered rods. The power transmission coefficient is then practically unity all along the rod, and reflections toward the feed are small and effectively cancel each other.

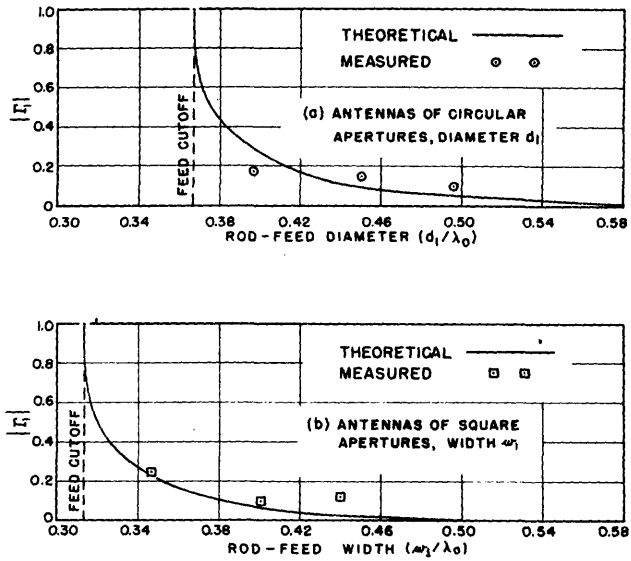


Figure 7 - Reflection coefficients at the rod-feed junction vs. rod-feed aperture, for uniform polyrods

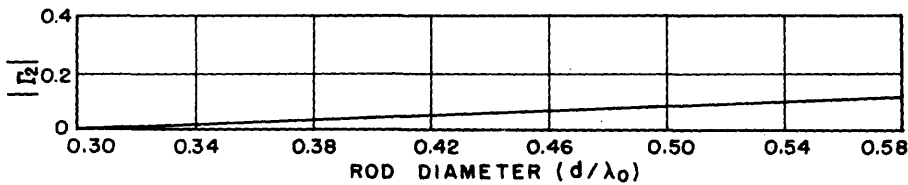


Figure 8 - Theoretical reflection coefficient vs. rod diameter at any point along uniform-taper polyrods

SCOPE OF THE EXPERIMENTAL WORK

The major portion of the experimental work consisted of aperture, tapering, and reinforcement studies of the end-fire radiators, and the electrical effects of mounting the scanning polyrod near flat aircraft fuselages.

Antennas for Toroidal Beams

Single dielectric rods and discs can be designed to yield toroidal beams. A beaded rod of stepped and multielectric form is under investigation by Mueller (11). This utilizes alternate sections of relatively high dielectric constant in order to obtain transverse directivity—varying the bead spacing controls the direction of the toroidal beam.

Figure 9 shows side views of the present and the contemplated models of disc-type antennas originated at this Laboratory. The polydisc antenna is a tapered dielectric disc conceived as analogous to a large number of polyrods arranged radially in a plane—the

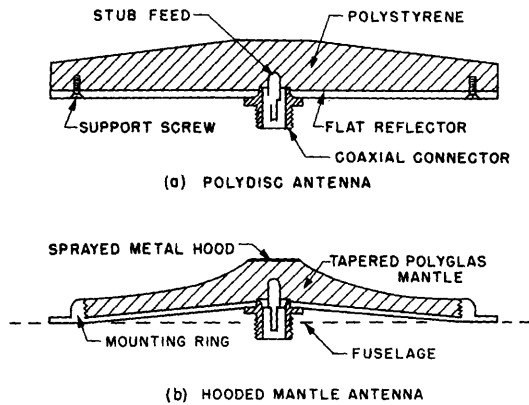


Figure 9 - Experimental toroidal beam antennas, section views

guided wave propagating radially along the disc, rather than in a single preferential direction. Very little work was done with the antenna though enough was accomplished to indicate promise of excellent performance as an airborne beacon antenna, yielding uniform radiation throughout a single plane or arbitrary surface. Especially in contrast to a conventional microwave beacon array of dipoles or slots, or to a biconical horn, the disc-type antenna is suitable for high-velocity aircraft because of the short projection from the fuselage and the gradual contour of streamlined shape.

The antenna affords convenient means of controlling the radiation of a stub feed toward the horizon. As the disc radius is increased the beamwidth of the horizon lobe sharpens, and the elevation angle decreases, probably much in the manner of Mallach's half-aperture rods (10). Conceptually, the beam elevation is also controllable by suitable shaping of the mounting plate.

Polydiscs were constructed according to the image principle at S- and X-bands, being $\lambda_0/4$ thick and having a radius of $1.4\lambda_0$ and $4\lambda_0$, respectively. The support plates were of radius $4.8\lambda_0$ and $4\lambda_0$ so that, in effect, the smaller model was working against a large fuselage. Much better results were obtained in this case, showing the importance of a large reflector and a small disc radius. Without tapering, the minor lobes were 6 db below the main-beam level, and the elevation angle of the main beam, as well as the beamwidth, were on the order of 20 degrees. The larger model yielded very low gain, many elevation lobes appearing above and below the antenna of greater power than the main beam. Tapering this model yielded some improvement. A ± 2 db variation from omnidirectional radiation was recorded in the horizontal plane even though the elevation beam was not smooth. Further work was discontinued at this point.

Although the hooded mantle antenna was not constructed, by analogy to the multiple-taper rods, it should yield lower minor lobes than the present polydiscs because of the rapid taper in the feed region, and the improved type of feed. The sprayed metal hood should perform as a parallel plate radial transmission line between the stub feed and the disc radiator, thereby reducing the excitation of higher order modes and suppressing the extraneous elevation lobes. The supporting ring should not affect the radiation appreciably.

End-Fire Radiators

Most of the rod-, tube-, and horn-type radiators listed in Figure 1 were constructed, and measurements of their performance indicated the superiority of the rod type for sharp beam radiation. Flaring the tubes in the manner of horns caused sidelobes to rise. Considerable work was undertaken to investigate the effects of tapering long rods (in order to reduce the sidelobe radiation) and the effects of several means of reinforcement. Metallic reinforcement proved feasible, as did wrapping the junction of the radiator and feed with dielectric material.

During the course of the work, it was evident that short rods and tubes of large aperture yield fair impedance match, directivity, and low sidelobes without the necessity of tapering. These types were not so thoroughly investigated as long rods, but the characteristics of several models are compared in Figure 10 and Table 2, where the symbols have the meanings previously set forth in Table 1.

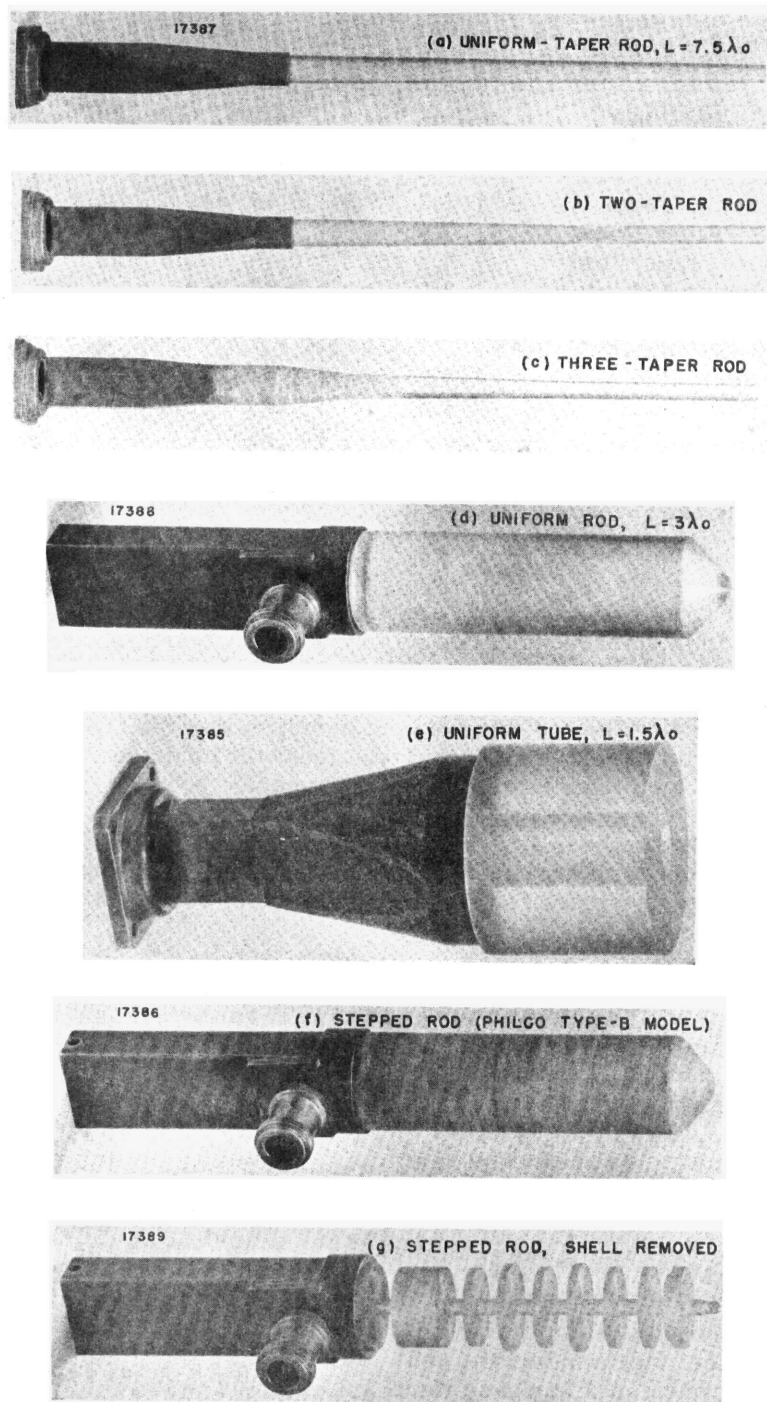


Figure 10 - Photographs of polystyrene antennas
(Characteristics listed in Table 2)

TABLE 2
Comparison of Polystyrene Antennas

Antenna	L/λ_0	l/λ_0	d_1/λ_0	G	BW	SL
GUIDE ANTENNAS						
Uniform-Taper Rod	7.5	7.5	0.45	17.4	21.5	-10.0
Two-Taper Rod	7.5	4.3	0.45	17.2	25.5	-15.8
Three-Taper Rod *	7.5	4.3	0.45	17.6	25.5	-19.5
Uniform Rod	3.0	-	0.85	6	52	-6
Stepped Rod	3.0	-	0.85	13	29	-12
LENS-GUIDE ANTENNAS						
Uniform Rod	1.5	-	1.8	14.9	30.5	-26
Uniform Tube †	1.5	-	1.8	16.4	26.5	-18

* Diameter over Fiberglas wrapping = $0.65\lambda_0$, $l' = 1.0\lambda_0$

† Wall thickness = $0.69\lambda_0$

Waveguide-fed rods of symmetrical aperture were constructed with a tapered dielectric section within a tapered metal guide to match the aperture dimensions and impedance of standard waveguide to those of the rod. A short uniform section of dielectric-filled metal guide provides internal support to the radiator. The antenna thus can be assembled by inserting the rod into the feed mouth so that the tapered surfaces fit snugly within. The many advantages of this type feed will be discussed later. Dipole- or probe-fed rods require no taper within the metallic cap.

Asymmetrical rods possess advantages for applications requiring an asymmetrical beam pattern, or for use with or without a side plate, as for scanning in a single plane. The designs illustrated in Figure 11 are representative of such applications, and their performance is considered subsequently.

Broadside arrays of end-fire radiators are attractive because of the small rod apertures (2) (4) (5) (7) (10). The element spacings of uniform arrays should be chosen so that nulls of the array factor correspond to the higher sidelobes of the individual rods. Sidelobes of long rods are so numerous as to make this operation difficult, so that in some instances fairly short rods are more feasible.

The effects of mounting rod antennas near metallic fuselages were also investigated.

GEOMETRIC PARAMETER EFFECTS

Before considering the design of rod radiators with assurance, certain factors contributing to the electrical performance were investigated. For this geometrical configuration study, a series of polyrods was constructed with the parameters shown in Figure 12.

The optimum dimensions of the uniform-taper rods were completely

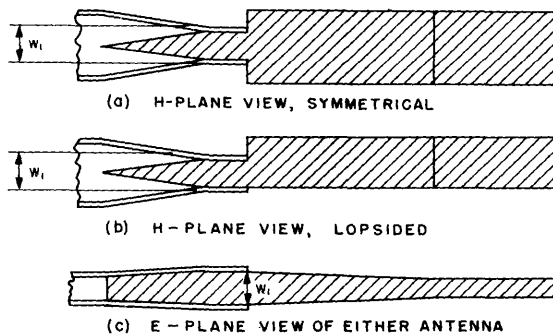


Figure 11 - Asymmetrical antennas, section views

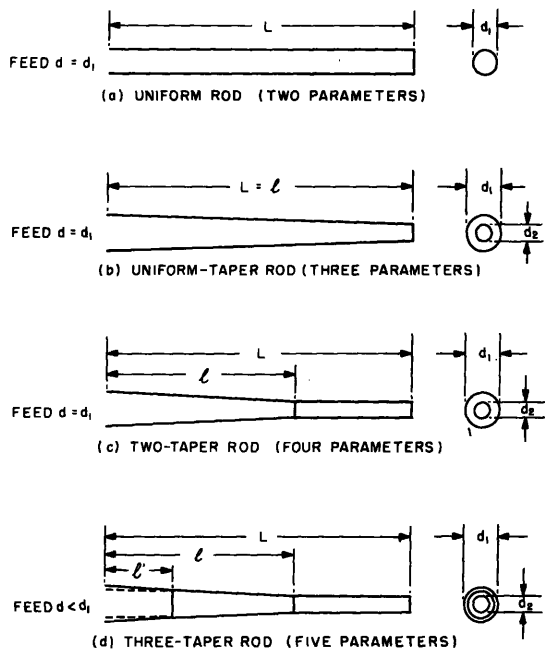


Figure 12 - Geometric parameters

determined, both for circular and for square apertures. The aperture criterion will be shown to hold, as well as the fact that circular and square apertures yield the same gain and radiation pattern. Corresponding data for one shape may be obtained from the other on the basis of $w = 0.886 d$.

The two-taper rods consist of the optimum uniform-taper rods (of the same feed and termination apertures) but with a more rapid taper of length l , followed by a uniform section, length $L-l$. Assuming the aperture criterion holds, the optimum dimensions are determined for two-taper rods.

The three-taper rods consist of the above two-taper rods wrapped along the rod-feed junction with Fiberglas, machined to shape. The aperture criterion was used for the termination, but not for the over-all thickness of the feed end. The optimum wrapped length, l' , is determined only approximately.

It may be noted that the most general forms of the two- and three-taper rods are specified by five and seven parameters, respectively, rather than four and five which are indicated. The method of investigation used here tremendously reduces the time required to obtain results satisfactory from an engineering viewpoint.

All tapers are linear, d or w decreasing linearly along the rod; and taper is usually specified by an area ratio, rather than an angle, so as to apply to any length and to either aperture shape. All dimensions are normalized to free-space wavelength to facilitate application at any design frequency. Thus for this study the fundamental parameters are:

Input Section Area	A_1 / λ_0^2
Taper Factor	A_2 / A_1
Radiator Length	L / λ_0
Tapered Length	l / λ_0
Wrapped Length	l' / λ_0

Aperture

Preliminary data using probe-fed polyrods were made to ascertain the optimum aperture areas A_1 and A_2 , which permitted the construction of a series of uniform-taper rods to investigate the effects of length and taper. Radiator main-lobe gain, beamwidth, and sidelobe suppression are not optimized at the same aperture (Figure 13). Sidelobes are lowest for small diameters, which afford low main-lobe gain. The best combination of gain and beamwidth for polystyrene is seen to be in the range of feed diameter, $d_1 = 0.42$ to $0.48\lambda_0$, verifying one part of the aperture criterion, $d_1 = 0.564\lambda_0 / \sqrt{e - 1} = 0.45\lambda_0$.

Figure 14 shows how the beamwidth and sidelobes are affected by tapering. The other part of the aperture criterion, $d_2 = \sqrt{0.4}d_1 = 0.29\lambda_0$, corresponds to an included taper angle $\psi = 2.3^\circ$ for $4\lambda_0$ conical rods, which is seen to be an effective compromise of the beamwidth and sidelobes.

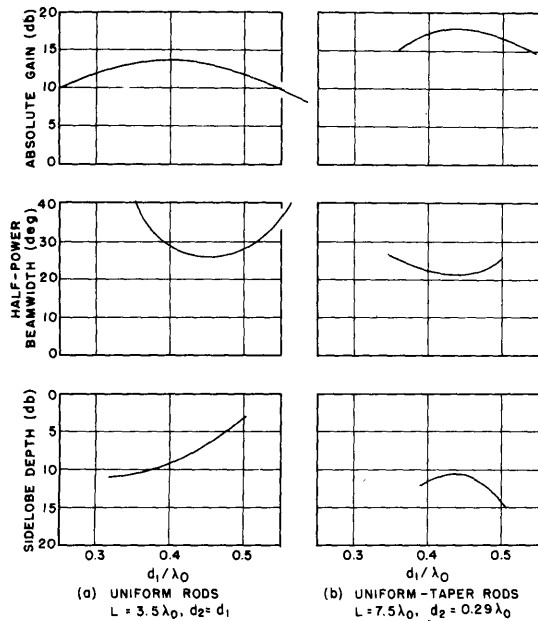


Figure 13 - Influence of polyrod aperture dimension for two radiator lengths

uniform-taper rods will suffice for some applications, but the long rods possess fairly high sidelobes which can be further reduced through the use of multiple tapers.

Tapers

Figure 18 compares uniform tapering of a long square-aperture rod tapered in two ways: one, by equal symmetrical tapering in the E- and H-planes, and two, by symmetrical H-plane tapering with no taper in the E-plane. The data indicates that tapering in the E-plane is more effective than in the H-plane. Curves in the E- and H-planes correspond to the more important phenomenon for radar, where maximum strength is a prime factor. The taper, $A_2 = 0.40 A_1$, is shown to result in maximum gain, sharp beamwidth, some sidelobe suppression, and increasing of the sidelobe angle. Curves in the E- and H-planes apply to either plane of polarization due to rotational symmetry near the main beam and to either square or circular aperture rods.

Figure 19 shows that the sidelobes of long rods are effectively suppressed by tapering rapidly from the feed end and following with a uniform extension. The amount of additional sidelobe suppression obtainable by this method varies with rod length, L , increasing from 1 db for $L = 3\lambda_0$ to 6 db for $L = 7.5\lambda_0$ (Figure 19 (c)). The optimum taper length, ℓ/λ_0 for minimum sidelobes, and the ratio, ℓ/L , both vary linearly with radiator length for $L > 3\lambda_0$, and the optimum ratio is plotted in Figure 19 (d).

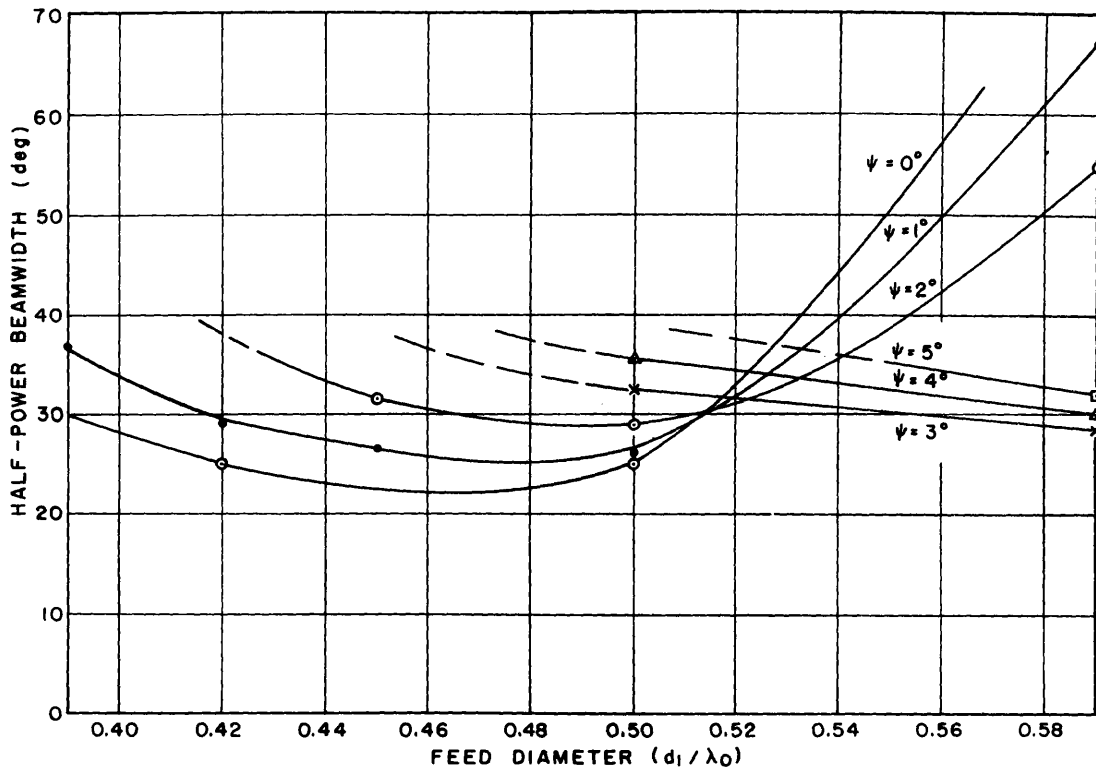
The gain (Figure 19(a)) and beamwidth (Figure 19(b)) characteristics of the two-taper rods are almost as good as with uniform tapering, $\ell/L = 1$, especially for the longer rods. Figure 20 and Table 2 (page 12) compare radiator performance of uniform and two-taper rods as a function of L/λ_0 . The aperture criterion was used for all these rods, the difference between the uniform-taper and two-taper rods being the rate of taper.

The foregoing experimental results were obtained for short uniform rods, $L = 3.5\lambda_0$, and for short and long uniform-taper, $L = 4$ and $7.5\lambda_0$, illustrating the feasibility of employing the aperture criterion in these ranges.

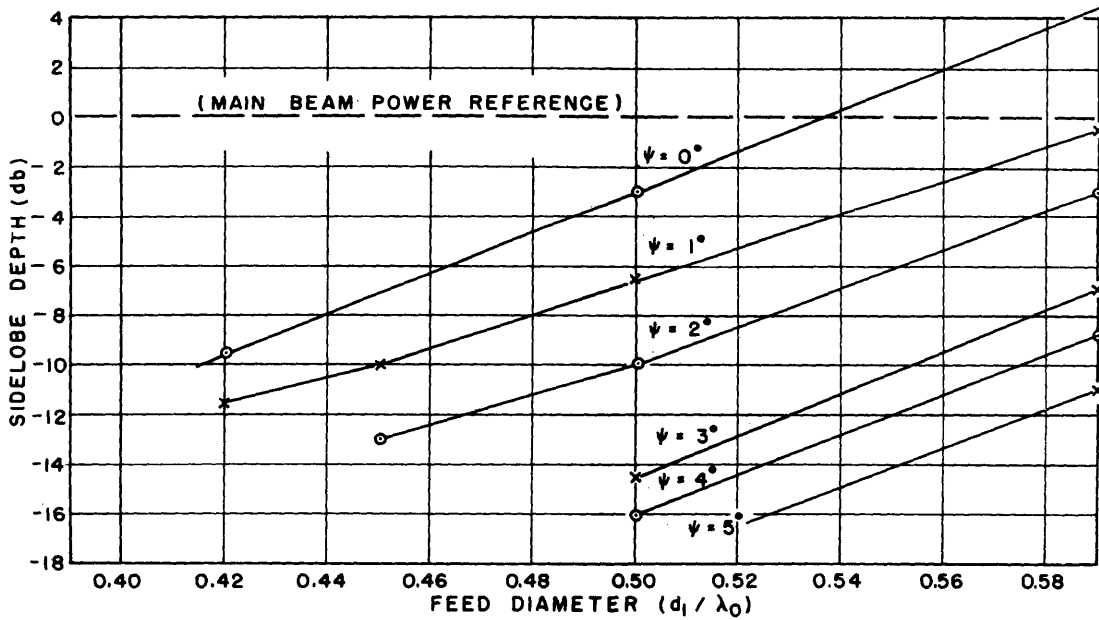
Figure 15 shows experimental data depicting gain, sidelobe depth, and beamwidth vs. radiator length for uniform-taper rods of the two aperture shapes. From this data, it is safe to say that radiation is relatively unaffected by minor variations in shape from square and circular apertures, since these apertures yield the same H- and E-plane field patterns and gain.

Length

Figure 15 presents the effects of radiator length upon uniform-taper rods designed according to the aperture criterion. The measured results were obtained with the subject radiators fed with the waveguide feeds indicated later in Figures 16 and 17. These



(a) EFFECT OF FEED DIAMETER ON BEAMWIDTH



(b) EFFECT OF FEED DIAMETER ON SIDELOBES

Figure 14 - Influence of feed aperture dimension and radiator taper for $4\lambda_0$ uniform-taper polyrods

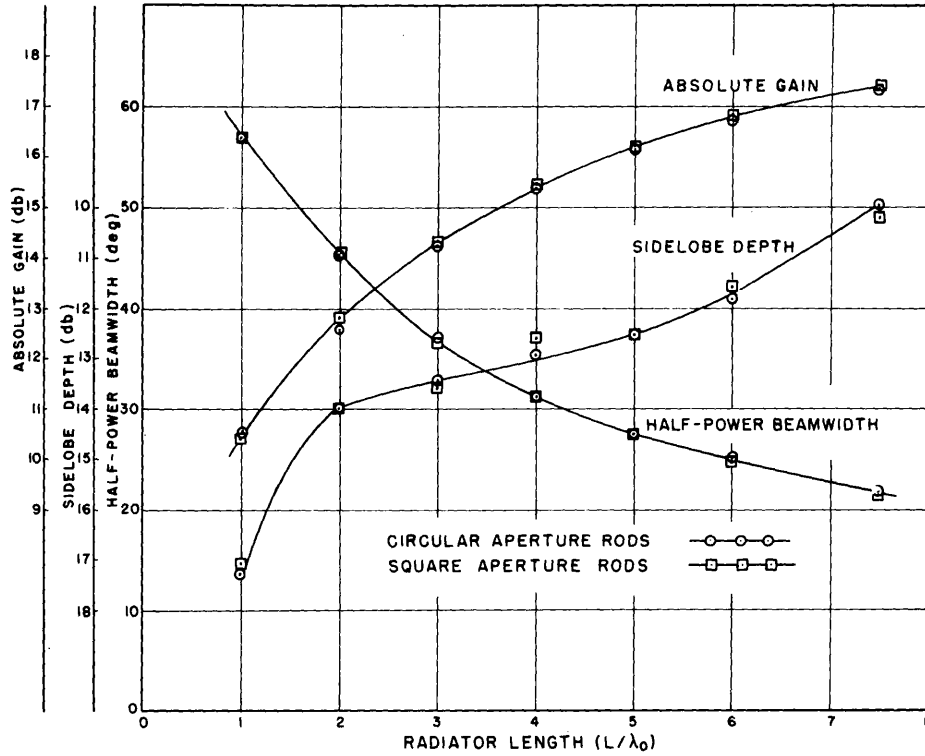


Figure 15 - Influence of aperture shape and radiator length upon uniform-taper aperture-criterion rods

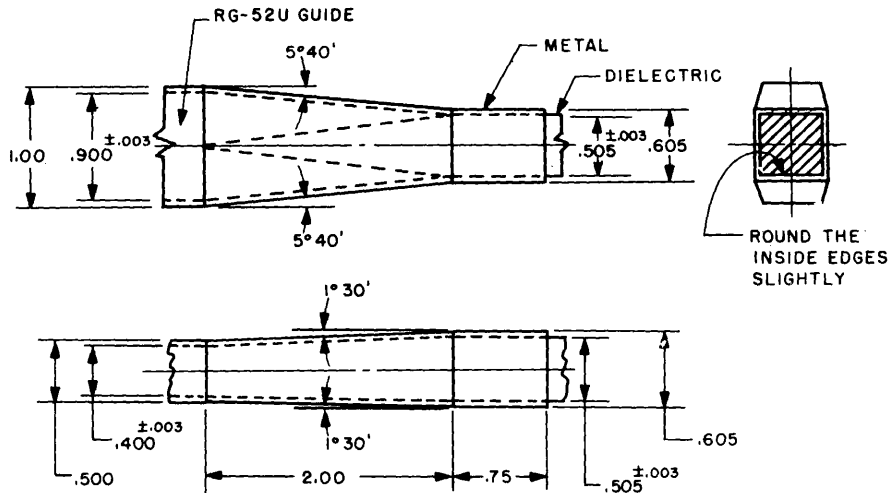


Figure 16 - Details of X-band waveguide feed assembly of square aperture

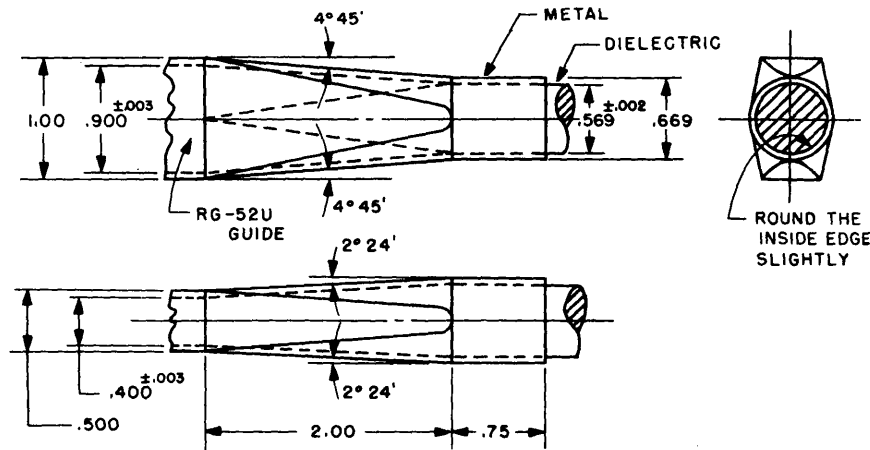


Figure 17 - Details of X-band waveguide feed assembly of circular aperture

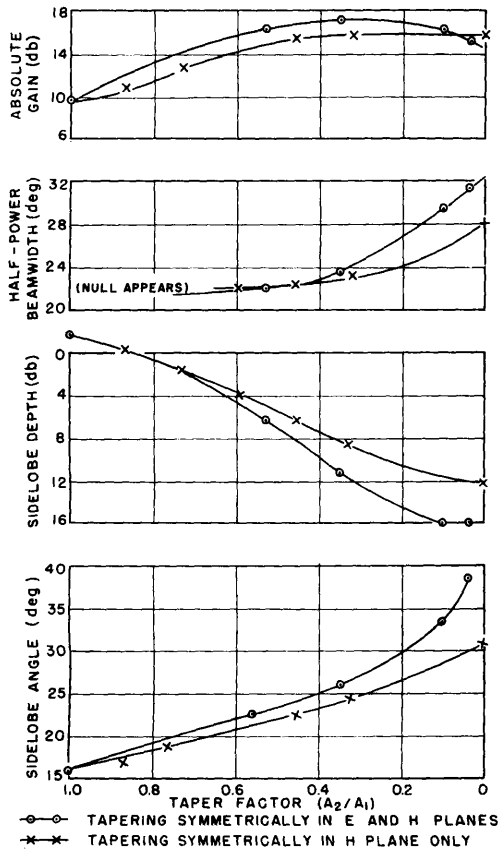


Figure 18 - Comparison of tapering a $7.5\lambda_0$ rod of square aperture in two ways

Sufficient data were not obtained to present completely the effects of l' and A_1 upon the characteristics of three-taper rods (Figure 12). With A_1 equal to $0.33\lambda_0^2$, the value of l' should be approximately $1.0\lambda_0$ to obtain minimum side-lobes (Figure 21). Excellent results were obtained for both circular and square apertures, the polystyrene rod aperture being enlarged relative to the feed aperture by Fiberglas wrapping. As a result of this work it is evident that the aperture criterion does not apply to the input aperture of rapidly tapered rods, but it may be used in designing the rod core.

Several rods were tapered from square aperture to round in order to combine the advantages of the square aperture feed and the circular aperture radiator (APG-18 (XN-1) experimental rod which was used for fuselage measurements). However, this resulted in slightly higher sidelobes than tapering without change in shape, due to the slow change of area along the feed end. There appears no reason why an abrupt change in shape as well as aperture area at the feed-radiator junction would not yield good radiation, such as using a square feed and an enlarged circular-rod input aperture.

DESIGN PRINCIPLES

From the foregoing theory, its experimental verification, and the experimental study of

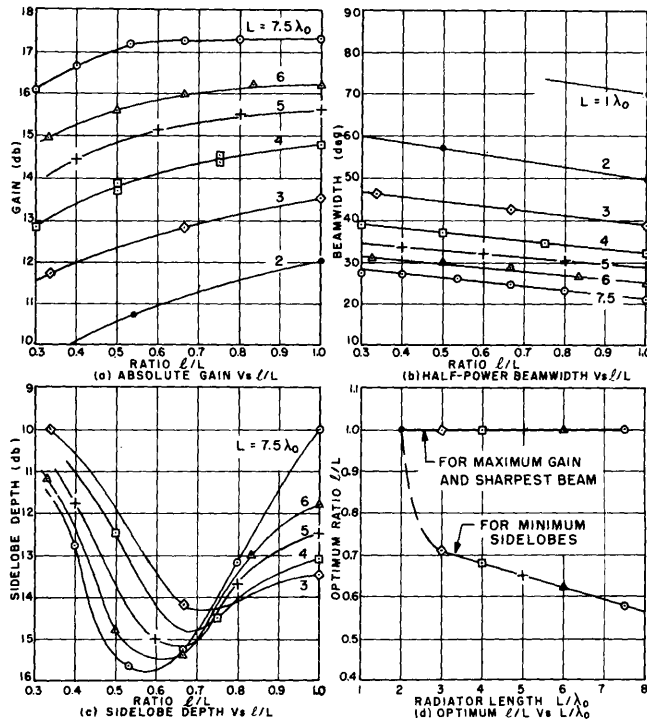


Figure 19 - Determination of optimum taper length l for two-taper aperture criterion rods

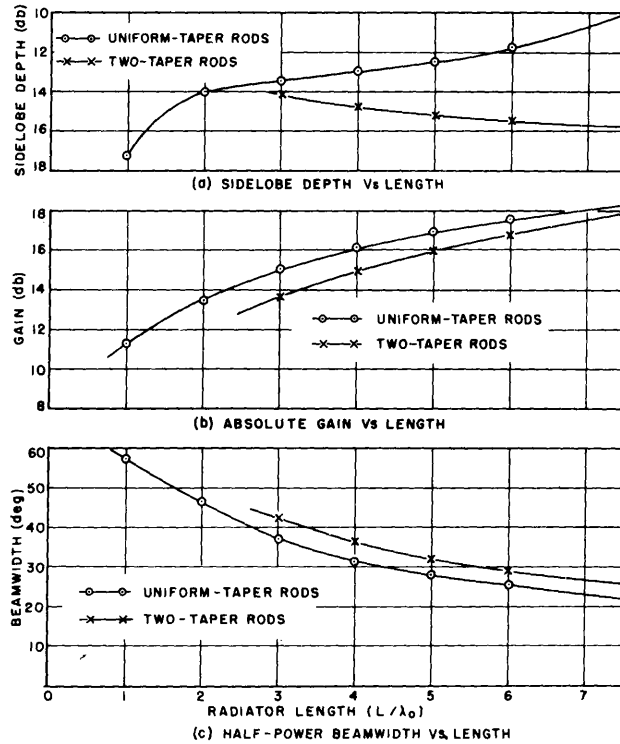


Figure 20 - Comparison of uniform-taper and two-taper rods of optimum dimensions

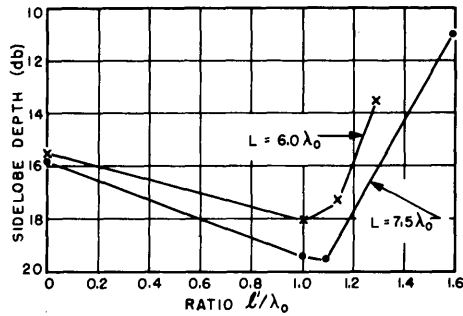


Figure 21 - Influence of wrapping length, L , upon maximum sidelobes in the H-plane for three-taper rods of over-all diameter $0.65 \lambda_0$, for two radiator lengths

the geometric parameters as they affect the performance of polyrod radiators, it is evident that dielectric rod design is a process of compromise between beamwidth, gain, and sidelobe structure in combination with aerodynamic strength features. All these are functions of radiator geometry as well as operating frequency, dielectric material, feed design, and reinforcement.

Design Frequency

No theoretical limitation exists for the application of dielectric-rod antennas throughout the radio spectrum. For aircraft, practical size limits the range to about 1000 to 60,000 megacycles, or 3000 to 10,000 megacycles for maximum directivity and use without radome protection. The

required ratio of radiator length to wavelength is increasingly realizable as the design frequency is raised.

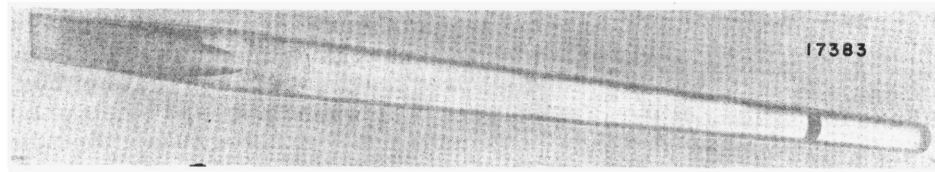
In order to reduce antenna weight and drag at the lower frequencies, the rod aperture may be shrunk by employing high dielectric-constant materials. However, this has no effect on the length required for a given directivity, and sometimes will weaken the radiator below the safe value, due to the large thinness ratio, L/d_1 . This may be overcome by shortening the rod, which results in reduced directivity. Another disadvantage of this approach is that antenna dissipation increases with dielectric constant. Therefore, the low-frequency limit is imposed either by insufficient strength or gain qualities. An array may be used in this case, but requires more lateral space. Performance improves as the design frequency is raised, until we reach such a high frequency that the thickness of the rod becomes very small even when employing the lowest dielectric-constant materials which may be used. Fabrication difficulties increase and the rods become too fragile to have any practical application, even when enclosed in a radome.

Dielectric Materials

Considering airborne applications, there is still need for a low dielectric-constant material of greater rigidity, and flexural and impact strength than is presently available. General airborne application requires that the physical and electrical characteristics hold under conditions of aircraft vibration, airstream pressure, and impact, throughout a wide temperature range.

Of the many dielectrics (17), very few possess the required characteristics of low dielectric constant, low power factor, and high strength. Plastics and ceramics best meet these requirements, some plastics affording high gain and fair strength, and some ceramics affording the reverse. Ceramics are generally used only below a frequency of 3000 Mc; plastics may be used at all microwave frequencies because of their inherently low dielectric constants.

Polystyrene, Dielectene, Fiberglas, Styramic and Lucite have been used in X-band model studies, with polystyrene yielding the best over-all performance. Figure 22 shows antennas of polystyrene and Fiberglas, illustrating their relative size. Table 3 indicates other materials which bear promise of somewhat greater strength, and characteristics of



(a) Circular aperture polyrod



(b) Square-aperture polyrod



(c) Square-aperture Fiberglas

Figure 22 - Photographs of aperture-criterion dielectric rods, $7.5 \lambda_0$ long at 9375 Mc

other materials (German) are published (9). The values of Table 3 are sufficiently constant throughout the microwave range to be used for design purposes. Cracking and warping often occur in the machining and reinforcement of polystyrene rods, and strain relief is difficult, thus molding is advisable for other than experimental models.

Since there is limited range of apertures which afford high strength and high gain, there exists a limited design variation for dielectric constant and power factor. Strength wise, it is desirable to feed and support the radiator with waveguide of aperture equal to that of the rod or the rod core. Especially at the higher design frequencies, this reduces structural strains in the dielectric at the rod-feed junction, conveniently allowing additional rod thickness to be obtained by Fiberglas wrapping. The feed guide must ensure single dominant-mode transmission, and allowing twenty-percent tolerance to the directive aperture area criterion, the range of dielectric constant is 1.8 to 12 for circular apertures, and 1.2 to 50 for square apertures. This is obtained by requiring that the cutoff ratio λ_0/λ_c be 0.77 to 0.90 in circular waveguide and 0.50 to 0.90 in square waveguide, corresponding to the larger bandwidth obtainable with the square guide. For optimum radiation, i.e., allowing no tolerance to the aperture criterion, the range of dielectric constant is 2.2 to 4.0 for circular apertures, and 1.3 to 5.3 for square apertures. These exact ranges (dielectric constant, Figure 23) are imposed solely because the rod core and feed apertures are made equal, to obtain maximum strength.

In addition, Mallach implicitly indicated by his phase-velocity criterion that radiation is more directive for dielectric constants no greater than 4. For the above reasons the lower constants are recommended except possibly at the lower frequencies, where weight may be reduced by the use of smaller apertures.

TABLE 3
Ceramics and Plastics for Antenna Design (17)*

Material	e	Tan δ	Flexural Strength (psi)	Strength Merit	Feed Dia. d_v/λ_0
Al Si Mag A-196	5.3	0.002	22,000	0.7	0.272
Porcelain (dry process)	4.8	0.01	-	-	0.289
Steatite 410	5.7	0.001	-	-	0.260
Tam Ticon MB	13.3	0.001	-	-	0.161
Amphenol No. 200	2.29	0.0028	-	-	0.496
Bakelite Resin	2.7	0.014	51,000	3.9	0.432
XRS-16631					
Glass Filler 55%	3.02	0.0070	25,000	1.6	0.398
Columbia					
Resin CR-149	2.51	0.0005	18,000	1.5	0.460
Dow Experimental					
Plastic Q-247	2.42	0.0005	-	-	0.474
E-Resin					
Fiberglas Laminate	3.78	0.013	25,200	1.2	0.338
ECC-11-148					
Lucite	2.57	0.003	15,000	1.25	0.450
HM-119					
Plexiglas	2.59	0.006	14,000	1.15	0.446
Polystyrene					
XMS-10023	2.55	0.0005	12,000	1.00	0.452

*All data applies to temperature of 25°C. Strength merit indicates relative strength of dielectric rods using these materials, i.e., S.M. = flexural strength/7,700 (e-1). Feed diameter is according to the aperture criterion.

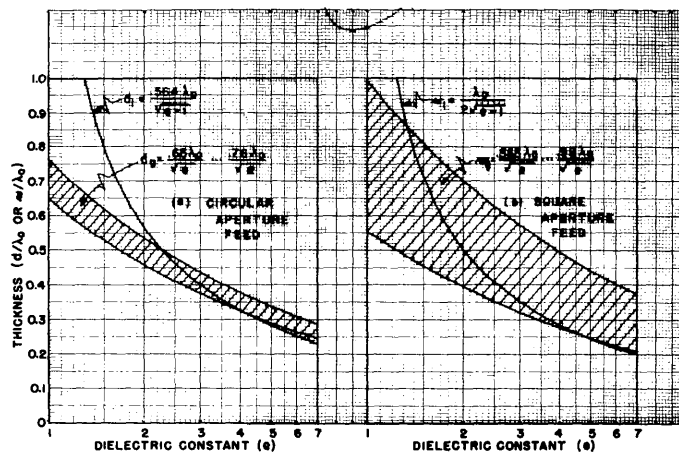


Figure 23 - The aperture criterion and the range of favorable feed dimensions vs. dielectric constant

Feed and dielectric dissipation must be minimized in order to maximize the gain. Figure 32, which will be introduced later, presents calculated absolute gain over a large range of parameters including dielectric constant and power factor.

In summary, the above design ranges of dielectric constant are imposed, firstly, because the rod core and feed apertures are made equal to afford maximum inherent dielectric strength, to facilitate dielectric wrapping, and to obtain the proper mode characteristics in the feed — and secondly, to obtain maximum gain irrespective of feed considerations, that is, a good compromise between the directive radiation of high constants and the low dissipation and the free-space matched radiation characteristic of the low dielectric constants.

Feed Design

In the lower uhf region, where a waveguide cap is too large, a probe feed without metallic enclosure might be used, providing the radiation effects of an alternate means of support are unimportant. For airborne purposes the source is enclosed by a metal cap or waveguide, the feeds of which conveniently support the rod and reduce back radiation. The capped probe or dipole is most convenient at 10 cm when coaxial transmission line is used, and the waveguide is better at 3 cm wavelengths.

Waveguide feeds were utilized in the majority of cases covered by this investigation, and the details of these feeds are shown in Figures 21 and 22. The aperture area and shape are chosen the same as the feed end of the circular (or square aperture) rods to obtain high strength, the optimum being determined by the aperture criterion to obtain good directivity. It will be found that the reflection at the feed-radiator junction is small. The circular form propagates only the dominant H_{11} mode, and the square form solely the dominant H_{10} mode.

These feeds possess the necessary taper sections to transform from standard rectangular X-band waveguide (RG-52/U) to polystyrene-filled circular or square feed sections. Dummy-load measurements of these feeds indicated negligible internal reflection, especially for the square form. The cutoff ratio λ_0/λ_c is 0.8 for each, and the aperture areas are equal.

Since the transformer section within the feed is electrically short, we may assume good transmission characteristics in the operation range from ten percent below cutoff wavelength for the dominant mode to one percent above cutoff for the second mode. On this basis, Figure 23 shows the dimensional range for circular- and square-aperture feed guides (d_g and w_g) over a range of dielectric constant. The radiator apertures (feed end, according to the aperture criterion) are superimposed for comparison. It is seen that in making the feed and rod apertures equal, good feed and radiation characteristics are simultaneously obtained over the favorable range of e , including the case of polystyrene $e = 2.55$.

Figure 24 illustrates two general methods for feeding closely spaced elements of two-dimensional arrays. The cascade type feeds the elements one after the other, so that the relative phases of the radiators are dependent upon frequency deviation and the phase constant of the line. The branch type feeds the radiators by means of branches of equal length, the line being branched once for each pair of radiators. Coaxial or waveguide line may be used in either method, application to the branch type being shown in Figure 25.

The branch type is best restricted to an even number of elements in either plane of polarization and becomes rather bulky when a large number of radiators are used. Coaxial line may be utilized in combination with waveguide to shorten the length of the feed as in Figure 25(b).

Advantages of the branch type for uniform arrays are: (a) design procedure is more simply calculable; (b) direction of the main beam does not change with frequency; (c) dissipation loads are not required; and (d) the choice of inter-element spacing does not involve altering the transmission line phase constant. The smallest spacing possible with standard hollow rectangular waveguide of the branch type is about $0.8\lambda_0$ in the H-plane and $0.5\lambda_0$ in the E-plane.

The cascade type (4) is recommended when a large number of elements are required, or when the relative phase of the elements are to be varied as for electrical scanning.

Array Design

For uniform arrays utilizing two elements in the plane of interest, a plot (Figure 26) of the power array factor $\cos^2(\pi s/\lambda_0 \sin \theta)$ in decibels vs. θ , the angle off-axis, facilitates prediction of array patterns over a large range of element spacings s/λ_0 . For arrays of n elements in the plane of interest, the corresponding array factor is $(\sin n x/n \sin x)^2$ where $x = \pi (s/\lambda_0) \sin \theta$, assuming radiators of equal phase and amplitude.

Table 4 illustrates the predicted pattern characteristics of several uniform arrays designed for sharpest beamwidth with arbitrary maximum acceptable sidelobe levels. This assumes that the measured sidelobes will be 0.5 db higher than theoretical in accordance with experimental data. This effect is caused by interaction of the rods as well as the large feeds. The larger spacings yield the sharper beamwidths, but too large a spacing may manufacture high sidelobes from the main-beam energy of the individual elements.

Considering only the elements in Table 4, we find that in order to obtain a beamwidth less than 14 degrees with -16 db sidelobes, or 17 degrees with -19 db sidelobes, it is necessary to use more than two elements in the plane of interest. It is significant that in the case of -16 db acceptable sidelobes, the array of $6\lambda_0$ two-taper rods yields sharper beamwidth than either type of array utilizing $7.5\lambda_0$ rods.

The radiation from arrays of four elements arranged two by two is rotationally symmetric, approximately. The array factor is almost independent of polarization in this case, but is increasingly dependent as the number of elements in a square array is increased.

Gain Considerations

Antenna gain is maximized by beam sharpening, sidelobe suppression, impedance matching, and choice of low-loss dielectrics. Methods of accomplishing these individually have been discussed. At least for $L > 3\lambda_0$ they cannot be effected simultaneously, and maximizing gain results in some broadening of the beam.

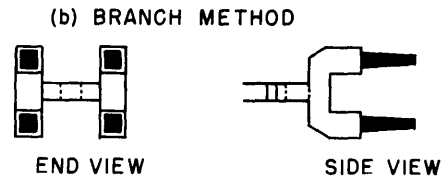
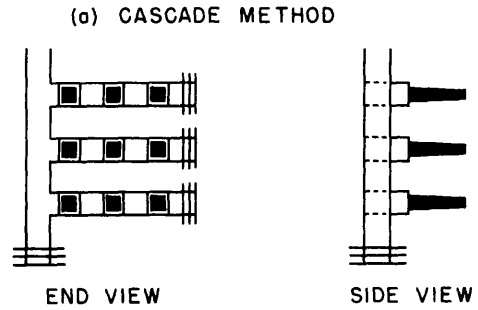
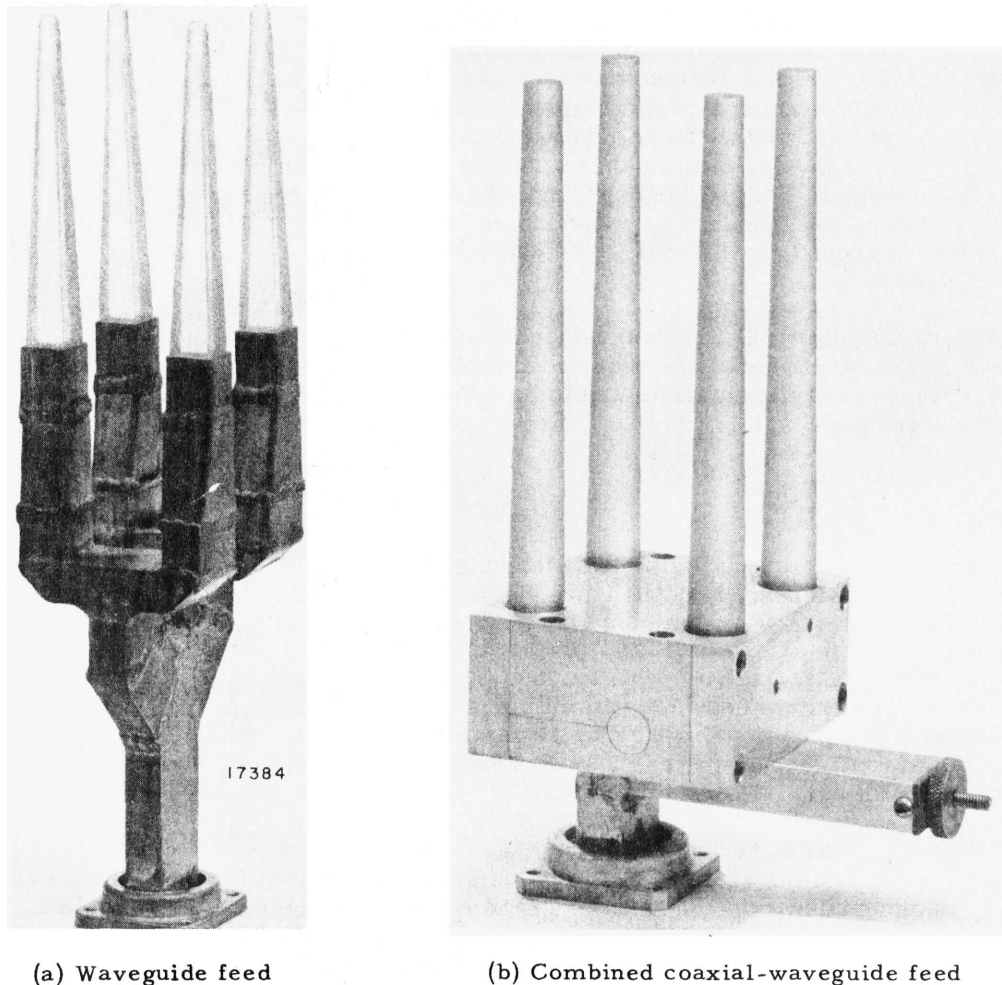


Figure 24 - Array feeds, cascade and branch



(a) Waveguide feed

(b) Combined coaxial-waveguide feed

Figure 25 - Photographs of four-element broadside polyrod arrays

Gain has been shown to increase with length for uniform, uniform-taper, two-taper, and three-taper rods. The uniform-taper and three-taper rods attain the highest gains, the latter yielding at least 17.6 ± 0.7 db (one-way measurement). Higher gains may be obtained with arrays, the power ratio increasing approximately as the number of appropriately spaced elements. In the event of aerodynamic failure, the three-taper rod should provide approximately 13 db gain since the Fiberglas section would remain in operation.

Beamwidth Considerations

Half-power beamwidth of uniform rods (medium length) is relatively sharp compared to tapered rods, but sidelobes are high. The beam degenerates to a null as the rod is lengthened or thickened. Tapering to reduce the sidelobes results in displacement of the nulls away from the beam, and consequently the beamwidth is broadened. It is impossible to optimize beamwidth and sidelobes simultaneously because of their inverse relationship.

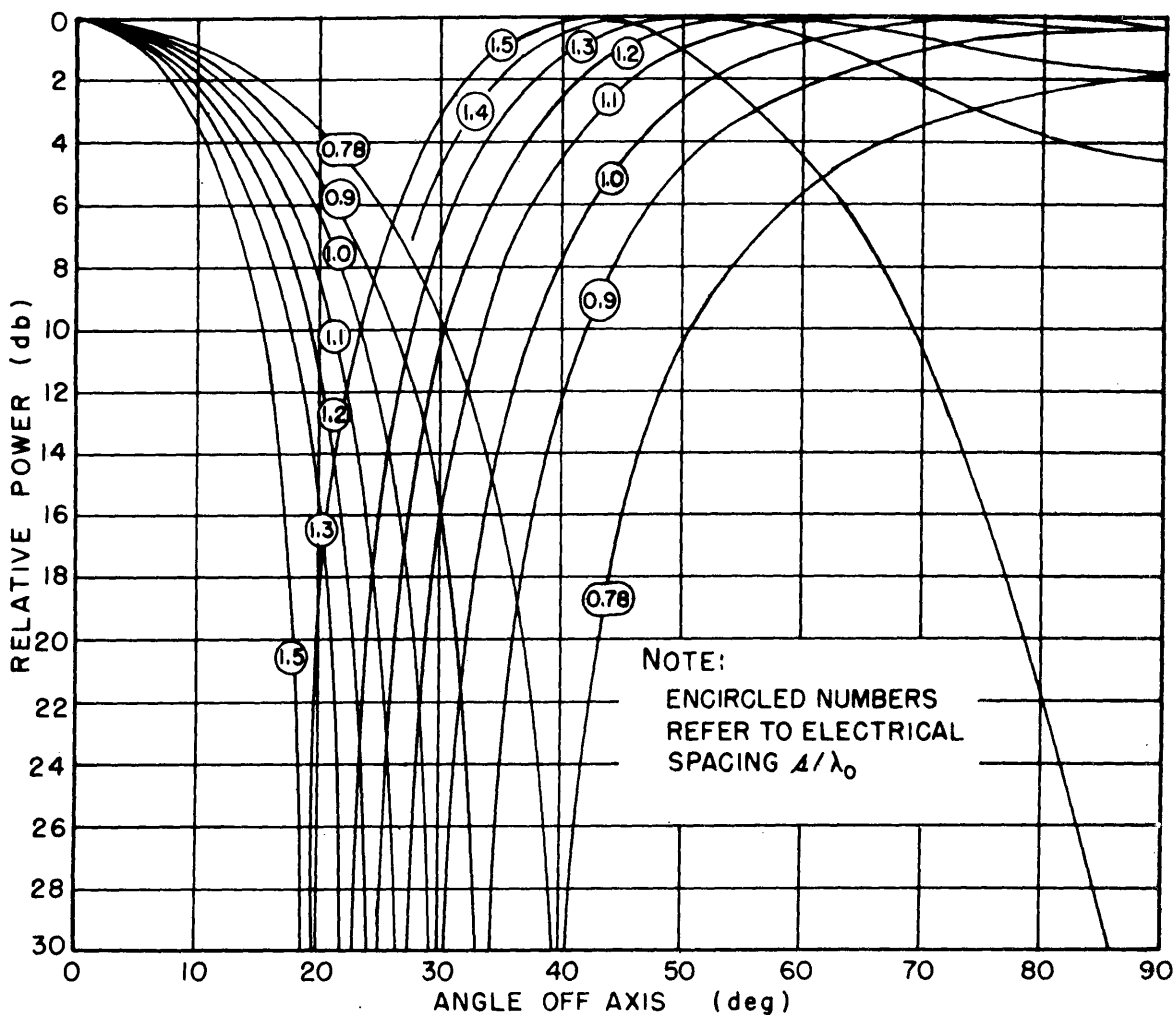


Figure 26 - Array factors for design of two-element broadside polyrod arrays

TABLE 4
Calculated Beamwidth and Element Spacing of Two-Element Polyrod Arrays
Designed for Sharpest Beamwidth at Arbitrary Maximum Acceptable
Sidelobe Levels

Type of Element	Radiator Length L/λ_0	Beamwidth and Spacing Required for Sidelobes			
		- 16 db		- 19 db	
		(deg)	s/λ_0	(deg)	s/λ_0
Uniform-Taper	7.5	15.8	1.27	17.0	1.03
	6.0	17.4	1.25	19.4	1.00
	5.0	19.1	1.20	21.7	0.95
	4.0	21	1.13	24.2	0.88
	3.0	24.4	0.99	26.6	0.87
Two-Taper	7.5	15.8	1.35	18.3	1.10
	6.0	14	1.7	19	1.05

The beamwidth of the aperture criterion rods sharpens with radiator length at least up to $7.5\lambda_0$, approaching 21 degrees for uniform-taper rods, and 25 degrees for the two- and three-taper rods. Sharper beams are obtainable with polyrod arrays, the half-power beamwidth in any specified plane sharpening approximately as the number of elements in that plane.

Sidelobe Considerations

Sidelobes and backlobes are substantial unless tapering is employed to decrease the aperture along the rod. The effects of several forms of taper have been discussed and depths approaching 20 db below the main beam were obtained for directive rods. It should be possible to lower this limit still further by exponential tapering, but with slight broadening of the beam as a sequence. With uniform tapering the sidelobes rise with radiator length, but for two-taper rods of $L > 3\lambda_0$ the reverse is true, sidelobes being somewhat suppressed by increasing radiator length. The 7.5λ rod yields -10 db sidelobes when uniformly tapered, -15.8 db sidelobes in the two-taper shape, and -17 db sidelobes for the three-taper version.

The above figures are the maximum sidelobes which appear, and in all cases these lie within 40 degrees of the axis, and the H- and E-planes are very nearly alike (rotationally symmetrical). In directions 40 to 90 degrees off axis, H-plane minor lobes are on the order of 2 db lower than those in the E-plane near 40 degrees, and 6 to 9 db in the region of 80 degrees. This characteristic was not measured for all designs, but apparently the H-lobes in this region are suppressed the more readily by tapering. Back lobes are usually 30 db down. Lower sidelobes are not necessarily obtained with uniform polyrod arrays, since extra lobes may be manufactured from the main beams of the elements.

Aerodynamic Factors

The strongest form of the dielectric radiator, for scanning purposes, is visualized as a hemisphere shape, whereas the most directive form is long and narrow. The rod is supported only at the feed end, as a cantilever beam, and stresses are induced in the dielectric due to the combined strains imparted by the slipstream, aircraft vibrations, and possible gun-blast pressures. Ultimate air-worthiness can be determined only by flight tests, because the structural characteristics of dielectrics—especially under impact loading of gun blasts—are not known throughout the required temperature range.

The stress calculations, Figure 27, apply only to the effects of aerodynamic drag upon circular-aperture polyrods in dry air of standard density. The drag and stresses are lower at higher altitudes. For materials of dielectric constant other than $\epsilon = 2.55$, the fiber stresses caused by drag may be approximated by $F_2 = F_1(\epsilon_2 - 1)/(\epsilon_1 - 1)$, since only the diameter of the rod is changed.

Figure 27 thus provides an estimate of the maximum fiber stress caused by drag upon microwave polyrods protruding into a transverse slipstream of velocity range 0 to 440 knots at sea level, corresponding to Mach numbers 0 to 0.65. This stress occurs at the end of the waveguide or rigid Fiberglass support, since the polyrod is loaded as a cantilever beam. The stress is $F = K_a C \delta (VL/d_1)^2$, where K_a is a dimensionless constant dependent upon the shape of the rod, C is the profile drag coefficient, δ is the air density in slugs ft^{-3} , V is the slipstream velocity in ft/sec , and L/d_1 is the thinness ratio. The results are practically independent of microwave frequency.

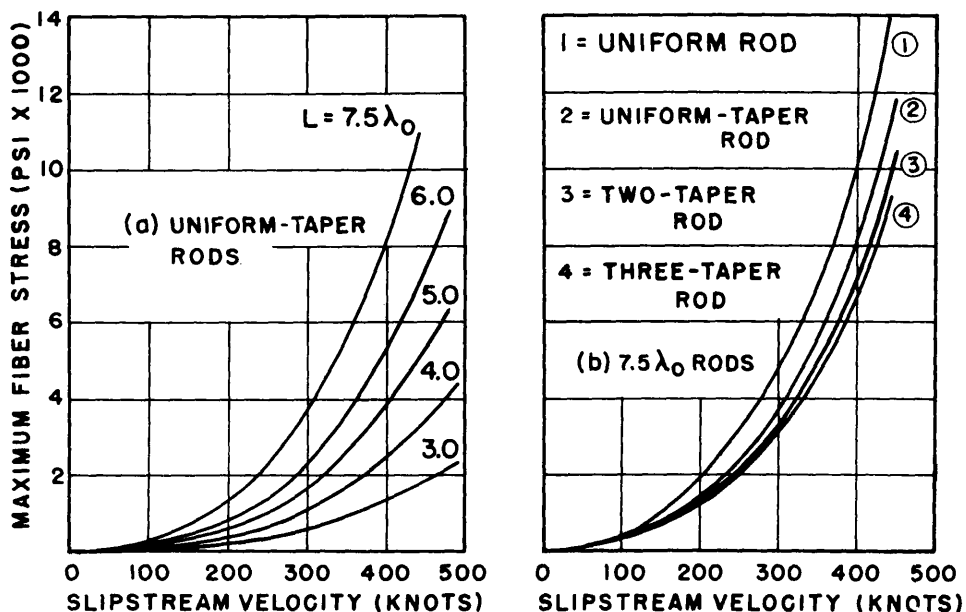


Figure 27 - Estimated maximum fiber stress in microwave circular-aperture

The $7.5 \lambda_0$ uniformly tapered rod (Figure 27) has yielded the sharpest beamwidth. This rod is subjected to a maximum fiber stress of 6000 psi at 360 knots, which has been assumed as a safe working stress of polystyrene until a more accurate figure becomes available. This value was obtained using a flexural strength rating of 12,000 psi with a working factor of two to include effects of aircraft vibrations and a safety factor. A low safety factor is recommended for wrapped rods because appreciable gain is maintained after rod failure—i.e., the break occurs at the end of the Fiberglas wrapping rather than at the end of the waveguide feed.

The maximum drag force imparted by the 360-knot slipstream for the X-band tapered rod is calculated to be 26 lb, indicating a power requirement of 0.008 hp to overcome the aerodynamic drag in scanning the antenna at 10 degrees per second at sea level.

The multiple-taper rods, according to calculations with or without the Fiberglas stiffener, appear to be adequate up to at least 380 knots velocity at sea level assuming the above working factor. The Fiberglas stiffens the rod so as to reduce deflection, rather than substantially decreasing the fiber stresses. Recent wind-tunnel tests at David Taylor Model Basin (22) resulted in the three-taper model deflecting at the tip in the amount of 1.8 inches prior to breaking at the end of the Fiberglas. The antenna withstood a dynamic pressure of 630.8 pounds per square foot, corresponding to Mach number 0.96 and a ram velocity of 591 knots air speed at 20,000 feet altitude (431 knots at sea level), NACA standard atmosphere. There was no metal insert in this rod, and the antenna was not vibrated in this test.

Vibration tests indicate the X-band polyrods without reinforcement are satisfactory for standard aircraft vibrations. A $7.5 \lambda_0$ antenna, constructed of styramic rather than polystyrene in order to exaggerate inherent structural weakness of the antenna, was

caused to break only at accelerations greater than those stipulated by the standard aircraft test (23). The rod finally broke at the rod-feed junction where the metal feed-aperture edges were not rounded as in subsequent models. Stress calculations show that this is the weakest portion of the antenna because of the cantilever construction, indicating the advisability of dielectric wrapping over this section for external-mount aircraft applications.

Square- and round-aperture rods possess greater strength under aerodynamic loading than asymmetrical shapes. Also, the strength of the square-aperture rods is one-half that of the circular at the most severe angle of attack, i.e., when the aperture diagonal is normal to the slipstream (8).

Pertinent weather characteristics include moisture absorption, surface water, icing, and temperature effects. Although dielectric losses are greatly increased, with consequent loss in gain, when moisture is absorbed, dielectric rods may be coated with a thin layer of water-proofing agent of low power factor. Polystyrene has negligible moisture absorption and adhesion is minimized with highly polished surfaces.

A thin layer of water or ice upon the rod surfaces will degrade the radiation characteristics. Measurements of gain upon $7.5\lambda_0$ square- and circular-aperture rods indicated losses in gain of 18 db and 9 db, respectively, with a maximum amount of water clinging to the surfaces. Flat surfaces allow the water to gather in puddles, which greatly increases the effective dielectric constant and loss. However, under flight conditions the effect should be negligible (9), because the airstream tends to maintain clean surfaces. Thin ice layers may adhere, altering the effective dielectric constant and breaking the rod because of the increased drag.

Single rods or broadside arrays of end-fire rods may be partially recessed within single- or multiple-slot turrets for hemispherical scanning, allowing only the dielectric to extend into the airstream. This is preferable to the use of a radome, providing the dielectric elements can withstand the consequent loading. Substitution of a two- or four-element array, of equivalent directivity, greatly shortens the antenna projection—thereby increasing the strength capacity. If a streamlined radome is used, the array substitution permits reduction in the required scanning space (radius), and the strength problem is solved at the expense of poorer radiation performance and greater drag upon the aircraft.

Reinforcement

Various methods of increasing the aerodynamic strength of the dielectric rod at X-band have been tried, as indicated in Figure 28 (a) and (b).

Figure 28 (b) illustrates a highly successful method, in which Owens-Corning ECC-11B Fiberglas tape is impregnated with Selectron 5003, wrapped snugly over the feed-rod junction in many layers, and dried by localized heating. The metal contact surface should previously be sand-blasted. The Fiberglas section is then machined along the rod for approximately one wavelength. The dimensions given in Figure 28 (d) were determined empirically and will be found to not only strengthen the rod junction but also to suppress sidelobe radiation.

The bending experienced by the rod under aerodynamic loading occurs most sharply at this junction before reinforcement. The wrapping eliminates the sharp discontinuity in rigidity through the junction and secures the internal support from loosening at low temperatures. The wrapping also serves as a pressure seal and should be coated to prevent moisture absorption.

Stiffening the remainder of the rod is best accomplished, in lieu of improved plastics or ceramics, with a thin metal septum or an I-beam laid symmetrically within the radiator

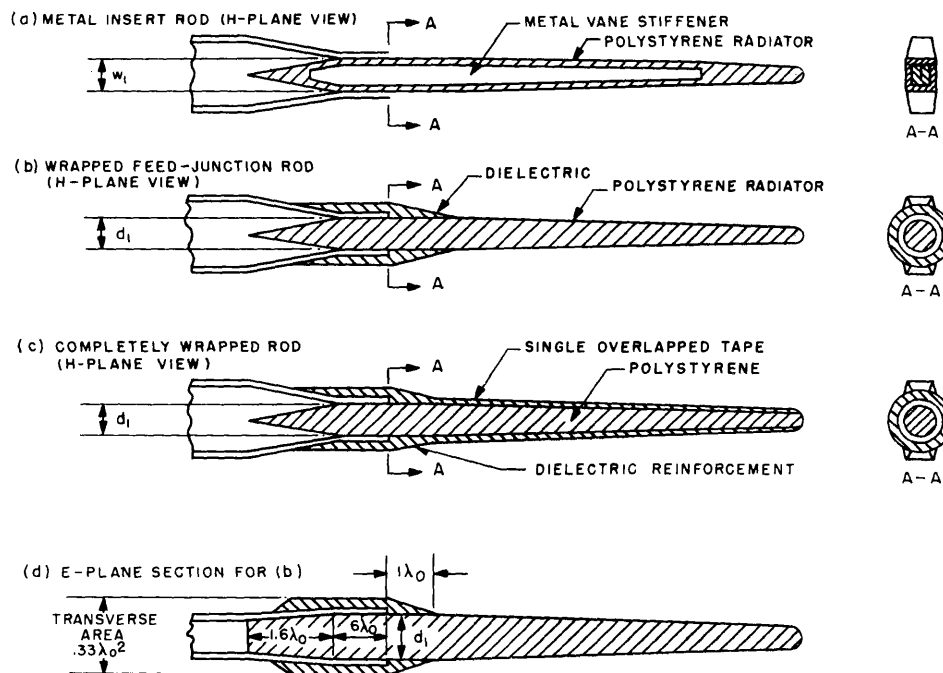


Figure 28 - Symmetrical reinforced antennas of square or circular aperture, section views

(in the H-plane of linear polarized antennas) as in Figure 28 (a). This degrades the gain and pattern only slightly. Successful fabrication is rather difficult unless the rod is molded. Complete Fiberglass wrapping of the radiator as in Figure 28 (c) is not recommended as the gain is appreciably reduced. However when dielectric tape of lower loss tangent becomes available, complete wrapping should greatly reduce the deflection of the rod at high velocities.

DESIGN PROCEDURE

The foregoing design considerations allow one to suggest the following steps to achieve a particular radiator design.

First, choose a dielectric material according to the desired frequency of operation. The characteristics of useful dielectrics are presented in Table 3 for application throughout microwaves. The work reported herein is chiefly X-band where, at the time, polystyrene proved to be the best choice of material. Other materials are available seemingly having advantages for radiators requiring greater flexural strength and rigidity at both S- and X-bands. At the lower frequencies a high dielectric-constant material may be used to reduce the antenna thickness and weight but not the length. For operation above X-band, no material is known which will provide appreciable strength for external mounting.

Second, choose the type antenna to be used according to the required characteristics of gain, beamwidth, and maximum acceptable sidelobes. Figures 20 and 21 give the characteristics of uniform-, two-, and three-taper rods to aid in this decision. Arrays are required to obtain gain greater than about 17.6 db, beamwidth less than 21 degrees plus maximum acceptable sidelobes below -10 db, and beamwidth less than 25 degrees plus maximum acceptable sidelobes below -20 db. Array design has already been discussed, and Figure 26

and Table 4 (page 25) will facilitate the procedure for the cases of uniform two-element arrays, or elements arrayed two by two.

Third, choose transverse dimensions at the radiator extremities according to the frequency and dielectric constant. Usually a circular or square shape is chosen, the circular possessing considerable strength and weather advantages, and the square allowing the use of more extreme frequencies. A design may be simplified and inherently strengthened by requiring that the rod and feed apertures be the same at this point of the procedure. The transverse dimensions may then be determined from the aperture criterion, as plotted in Figure 29. For the three-taper type, high-strength, low-loss tape will be wrapped along the rod-feed junction, and dimensioned as discussed previously.

Fourth, choose a feed aperture identical with the rod. For maximum strength the feed will be similar to one of the forms which were detailed in Figures 16 and 17. These feeds provide fairly good inherent matching, but may be matched more closely, at 9375 Mc for example, by use of an inductive iris placed 1.925 inches from the flange toward the load (square aperture), or 1.957 inches (circular aperture). The square feed provides slight size, bandwidth, and power-capacity advantages. Either feed may be shortened by about 1.5 inches at this frequency, $\lambda_g = 1.76$ inches in RG-52/U guide.

Fifth, choose a radiator length according to gain and pattern requirements. Predicted gain, beamwidth, and sidelobes for polyrods are given in Figures 20 and 21, which assume the rod will be dimensioned for maximum directivity consistent with minimum beamwidth (Figure 20) or minimum sidelobes (Figures 20 and 21) whichever is more important. For other materials the predicted gain may be obtained from Figure 30 which corrects for the change in over-all dielectric dissipation.

It is assumed (Figure 30) that antenna gain may be predicted for uniform- and two-taper rods of other dielectrics according to the data obtained with polystyrene rods—knowing the radiator length, dielectric loss tangent, and dielectric constant. Over the microwave range considered, the figure shows the characteristics of directivity and antenna losses. To illustrate the method, consider the uniform-taper solid Fiberglas rod, $L = 7.5\lambda_0$, $\tan \delta = 0.016$, and $e = 3.7$. The predicted gain according to Figure 30 is

$$\begin{aligned} G &= P - (\alpha_r + \alpha_f) \\ &= 17.7 - (3.0 + 0.3) \pm 0.7 \\ &= 14.4 \pm 0.7 \text{ db} \end{aligned}$$

This checks the measured absolute gain, $G = 14.4 \pm 0.7$ db.

Sixth, choose a taper length (l) according to the radiator length (Figure 19), if the two- or the three-taper form is chosen.

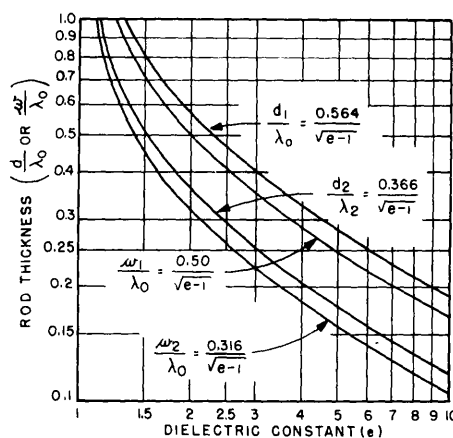


Figure 29 - The aperture criterion for design of circular or square aperture rods

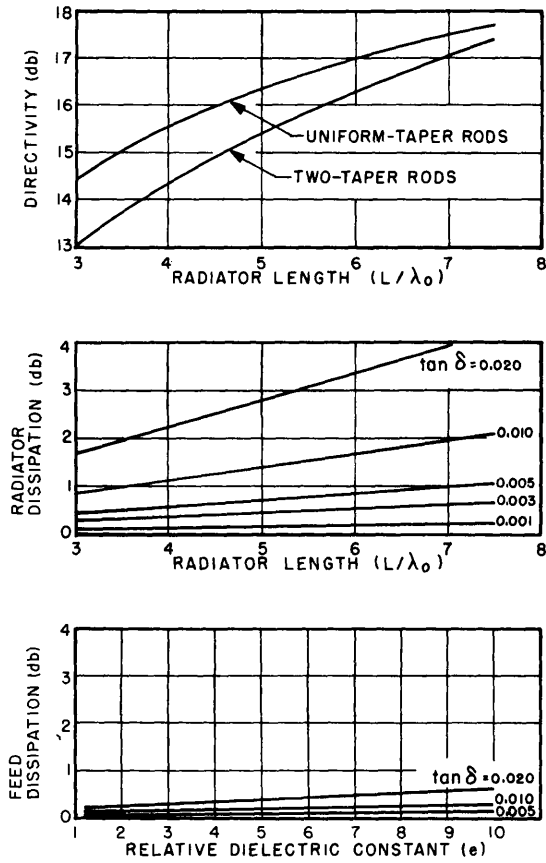


Figure 30 - Data allowing gain prediction for uniform-taper and two-taper dielectric rods

As the length or aperture area is increased above optimum the following progression is noticed. The sidelobes approach the main beam, both in magnitude and direction, the first sidelobes merge with the main beam and finally a null appears dead ahead. This final stage is an indication that the antenna contributes out-of-phase energy in this direction. Further enlargement alternately causes maxima and minima on axis, additional sidelobes are formed and continue to rise, and the gain alternately rises and falls. Apertures and lengths smaller than optimum cause beam broadening and lowering of gain (Figure 5).

There is an optimum inverse relationship between aperture and length for short uniform rods. Uniform rods of length $L > 3\lambda_0$ are normally not useful because of the high sidelobes and low gain obtained with reasonably large apertures.

Uniform-Taper Rods

Linear tapering (diameter or width) according to the aperture criterion resulted in the best designs for single rod applications where sharp beamwidth is more important than low sidelobes (Figure 32). These patterns apply to the H-plane for either circular or square shapes, but apply only to within ± 40 degrees for E-plane radiation. Beamwidth sharpens more rapidly with length than the rate of minor lobe rise, resulting in rising gain with length.

Seventh, choose a method of strengthening, if required. The aerodynamic strengths of polyrods of various lengths and forms are estimated (Figure 27) for speeds of 220 to 580 knots at sea level. The Fiberglas wrapping technique (Figure 21) is recommended as it further reduces the sidelobes, assures gain after rod-failure, secures the rod-feed junction, provides a pressure seal, and stiffens the rod, all with simple means of fabrication. Long rods may require internal I-beams or a very thin layer of reinforcement tape over all. Another solution is the use of a radome to protect the rod, or rods, from action of the wind stream.

FREE-SPACE MEASUREMENTS

Tapered rod antennas were constructed in several lengths and the following sections give the results of measurements of electrical performance, including radiation patterns, gain, beamwidth, sidelobes, impedance, power capacity, bandwidth, and polarization. Other antennas of interest are included. The technique used in making these measurements is described in the Appendix.

Uniform Rods

The uniform dielectric rod possesses unnecessarily high sidelobes as shown in the patterns of Figure 31, and others not shown.

According to the aperture criterion, polyrods are tapered from $d_1 = 0.45\lambda_0$ to $d_2 = 0.29\lambda_0$, or $w_1 = 0.40\lambda_0$ to $w_2 = 0.25\lambda_0$.

Figure 33 shows the effect of aperture shape and dielectric material upon the $7.5\lambda_0$ aperture criterion rod. Patterns are identical for all lengths of the circular- and square-shaped rods. The Fiberglas rod ($e = 3.7$) yielded approximately the same pattern except for the effects of greater dielectric dissipation—greater beamwidth, higher null level, lower sidelobes, and lower gain.

A comparison of patterns (Figure 34) of the $7.5\lambda_0$ aperture-criterion polyrod with rods of smaller and larger input dimension shows the beam is slightly broader in the latter cases, and the gain is lowered even though the sidelobes reduce.

Owing to tapering the $7.5\lambda_0$ polyrods to a point (Figure 35), both H- and E-plane pattern the beam broadens more rapidly than the minor lobes are lowered, so that the gain lowers. The data show that complete linear tapering does not lower the highest sidelobes in either plane of polarization very greatly compared to multiple or exponential tapering. In the region of 40 to 90 degrees off-axis, the sidelobes in the E-plane are somewhat higher than in the H-plane.

Tapering the polyrod is mainly useful in controlling the sidelobe level (Figures 31, 34, and 35). Zero taper yields high sidelobes and a minimum in the main beam of the long rods—tapering reduces the sidelobes and eliminates the main beam minimum, much in the manner of reducing either the aperture or the length of uniform rods.

Other patterns, which were interpreted in Figure 16, prove that tapering in the E-plane is more effective than tapering in the H-plane—information which is useful in the design of asymmetrical rods. These data also prove that rod radiation is a function of aperture area rather than rod dimension in either the H- or E-plane alone—i.e., tapering in either polarization plane is somewhat effective in controlling both patterns rather than either one independently.

Two-Taper Rods

Using the aperture criterion for a short portion of the radiator length followed by a uniform extension for the remainder results in a two-taper rod—the initial portion being more rapidly tapered than the uniform-taper rod, and the final portion being of zero taper. Patterns for several ratios of taper length to radiator length (Figure 36) show that rapid tapering greatly suppresses the high sidelobes and broadens the beam. An optimum value of taper length was shown in Figure 20, but of course this depends also upon the particular application.

Three-Taper Rods

Wrapping the radiator-feed end with Fiberglas, gradually tapered into the polyrod, greatly affects the radiation. If the dimensions are properly chosen, substantial minor-lobe suppression with negligible beam broadening is obtained. Only one value of over-all aperture was tried, for which the optimum wrapped length was determined for two radiator lengths, $L = 6.0$ and $7.5\lambda_0$ (Figure 37). In the event this type of rod were to break at the end of the Fiberglas wrapping, a short section of the rod would remain in operation. Though not measured, the gain and radiation pattern should be roughly equivalent to those of the $2\lambda_0$ uniform-taper rod.

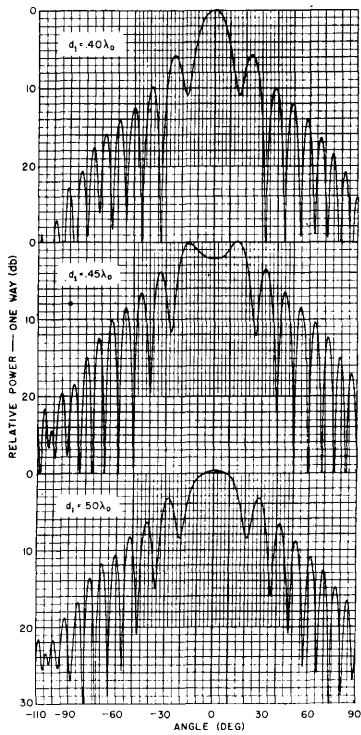


Figure 31 - Patterns of uniform polyrods, H-plane, $L = 7.5\lambda_0$, showing influence of aperture dimension

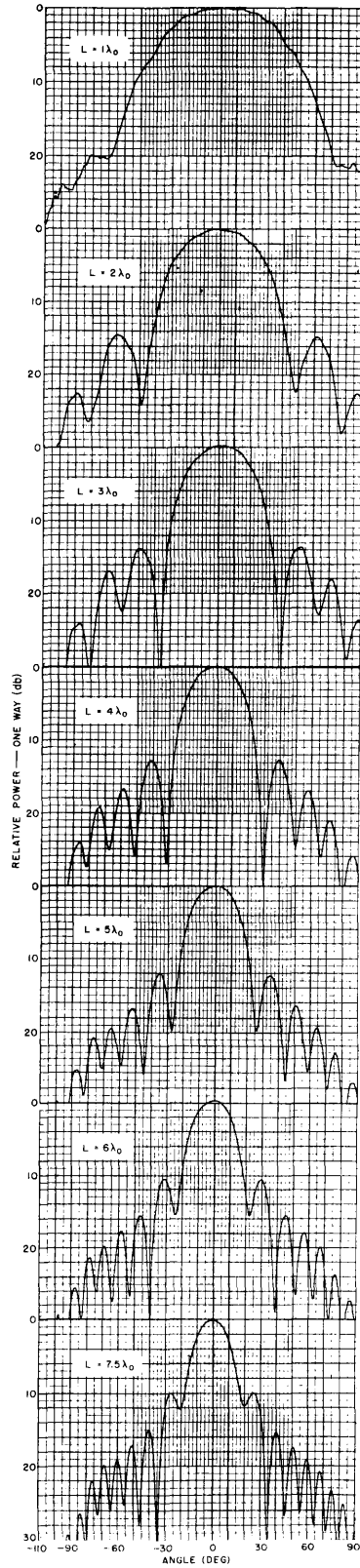


Figure 32 - Patterns of uniform-taper polyrods, aperture criterion, H-plane, showing influence of radiator length

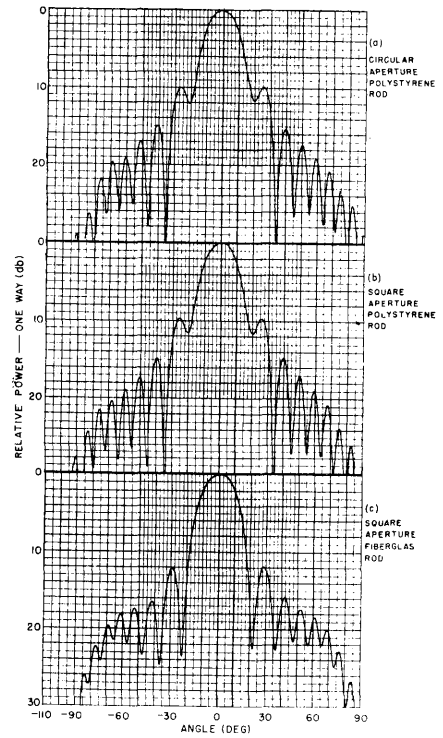
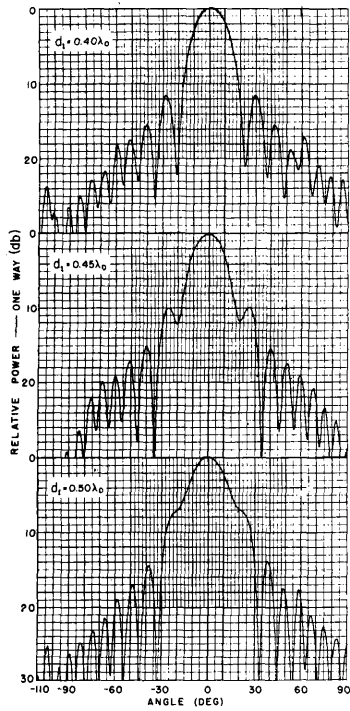
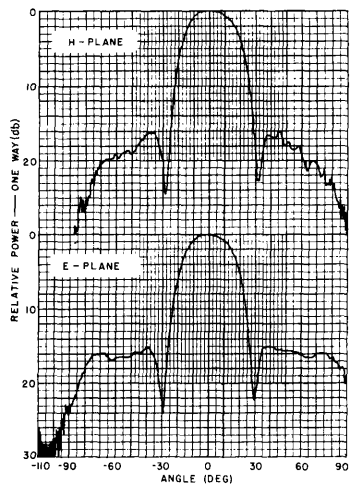


Figure 33 - Patterns of uniform-taper rods, aperture criterion, H-plane, $L = 7.5\lambda_0$, showing influence of aperture shape and dielectric material

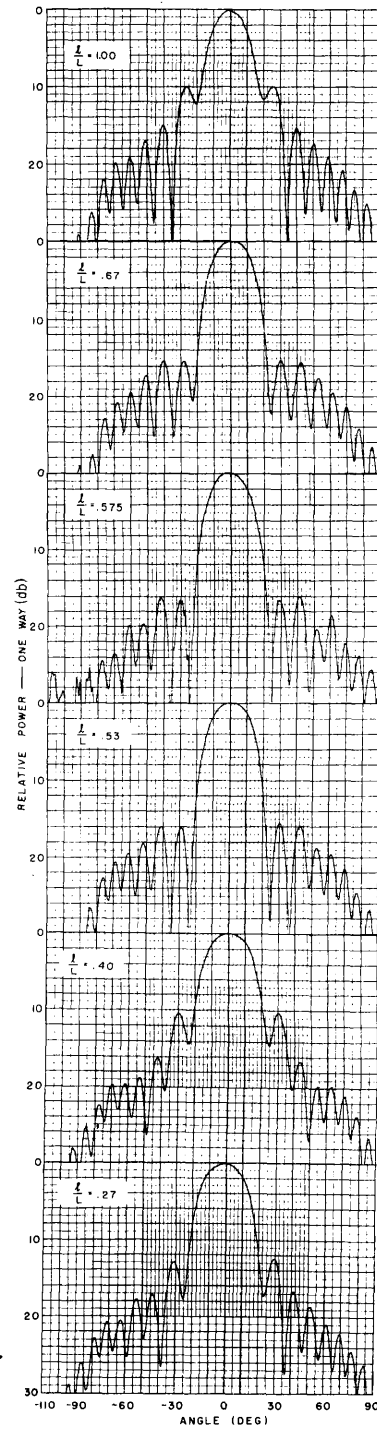


← Figure 34 - Patterns of uniform-taper polyrods H-plane, $L = 7.5\lambda_0$, $d_2 = 0.29\lambda_0$, showing influence of feed aperture



← Figure 35 - Patterns of a uniform-taper polyrod tapered to a point

Figure 36 - Patterns of two-taper polyrods, aperture criterion, H-plane, $L = 7.5\lambda_0$, showing influence of taper length



Asymmetrical Rods

It was previously mentioned that polyrod tapering in the E-plane is more effective than in H-plane of polarization. Therefore attempts were made (Figures 11 and 38) to taper large aperture rods only in the E-plane, utilizing the H-plane dimensions to obtain an asymmetrical H-plane pattern such as the cosecant-squared type. This idea was not carried to experimental completion.

The E-plane patterns are not included as the main-beam effects were comparable to those of polyrods having the same E-plane dimensions. Two of the H-plane patterns are shown (Figure 38), which illustrate that some control of pattern shape may be effected. The rod (Figure 11 (a)) yields asymmetry (Figure 38) when only one side is metallicly covered—but high sidelobes result. The lopsided form without a metal sideplate (Figure 11 (b)) yields a more gradually sloped main lobe. The latter antenna is interesting especially since the sidelobes in the E-plane are 16 db below the main beam.

Tubes and Stepped Rods

Figure 39 shows the effect of drilling a $0.4\lambda_0$ hole concentrically through a short thick uniform rod. This tube antenna (7) obtains directivity by virtue of both aperture and length, and might be considered as a circular broadside array of uniform rods. The effect of the hole is to raise the gain, sharpen the beam, and raise the sidelobes and back lobes. The characteristics (Table 2, page 12) are comparable to those obtainable with tapered rods, and the antenna is stronger than tapered rods of equivalent beamwidth.

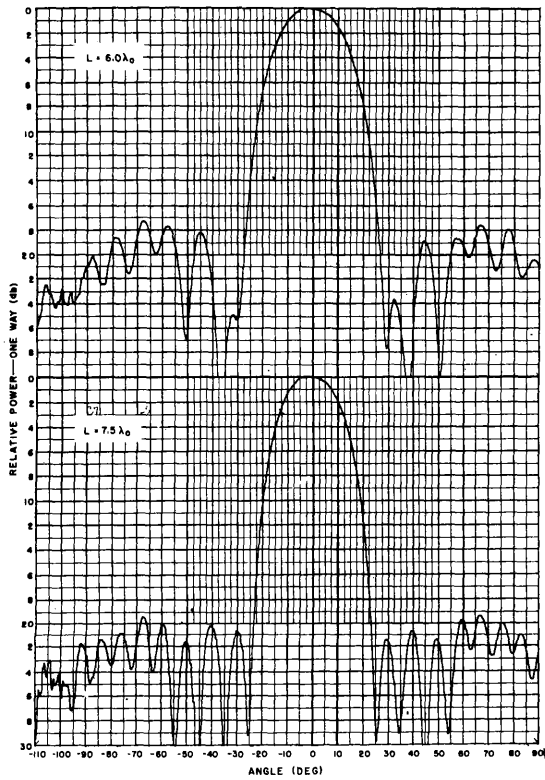
An X-band model of an S-band Philco Type B Antenna was constructed with the results given in Table 2. A core consisting of alternate sections of various diameters and thicknesses was supported by a thin-walled external dielectric tube. Owing to the large diameter of low effective dielectric constant, fairly sharp beamwidth was obtained for the short radiator-length tested. However, the sidelobes were higher than for tapered homogeneous rods of the same beamwidth, and no particular advantage is evident in this antenna.

Arrays

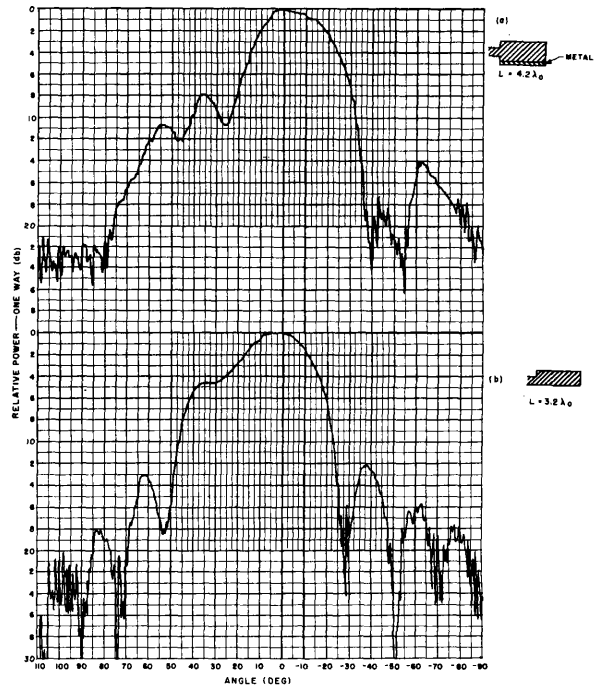
Figure 40 shows a pattern obtained with the second array (Figure 25) having four elements arranged two by two in the principle planes of polarization. The sidelobes are high because of the large spacing of $1.5\lambda_0$ between the elements, and measured 0.5 db higher than theoretical for one array and 2.5 db for the other. The measured gains were, respectively, 2.6 and 3.0 times those of the individual rods, but would be higher when properly matched. The beamwidths were accurately predictable by theory and the H- and E-plane patterns of the main lobe and maximum sidelobes were equivalent.

Impedance

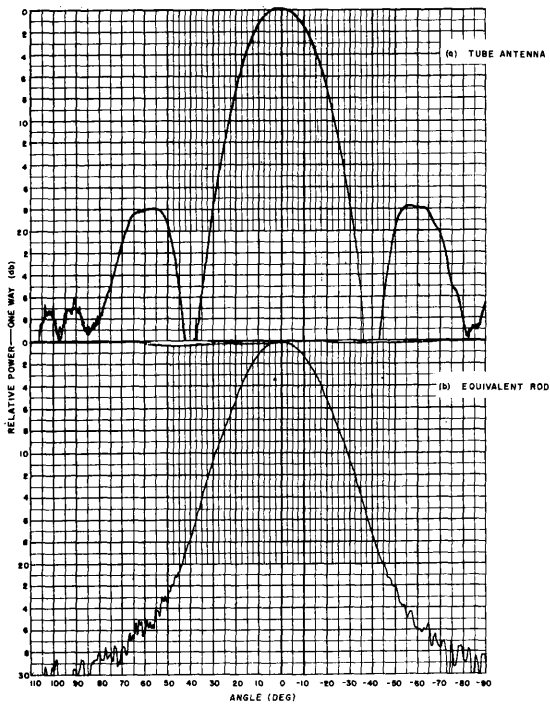
Input impedance measured at the waveguide flange for square and circular section tapered rods changes very little with radiator length (Figure 41) and is substantially resistive.



← Figure 37 - Patterns of three-taper rods with Fiberglas wrapping, H-plane



↑ Figure 38 - Patterns of asymmetrical rods, H-plane



← Figure 39 - Pattern of a short ($L = 1.5\lambda_0$), thick ($d = 1.8\lambda_0$) tube with $0.4\lambda_0$ dia. hole and comparison pattern of solid rod

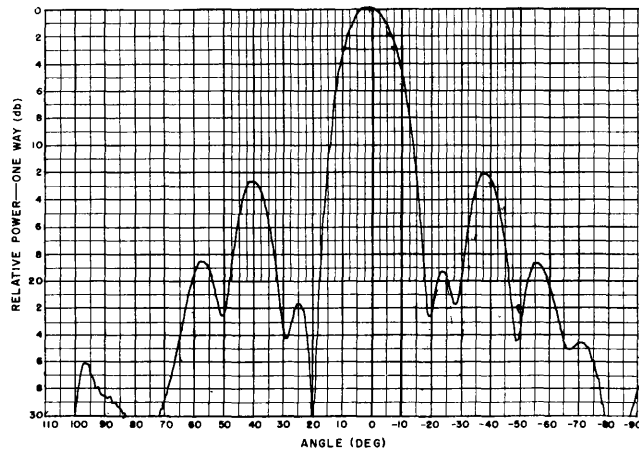


Figure 40 - Pattern of a four-element array, uniform-taper polyrods, arranged two by two $L = 4\lambda_0$, spacing = $1.5\lambda_0$, E-plane

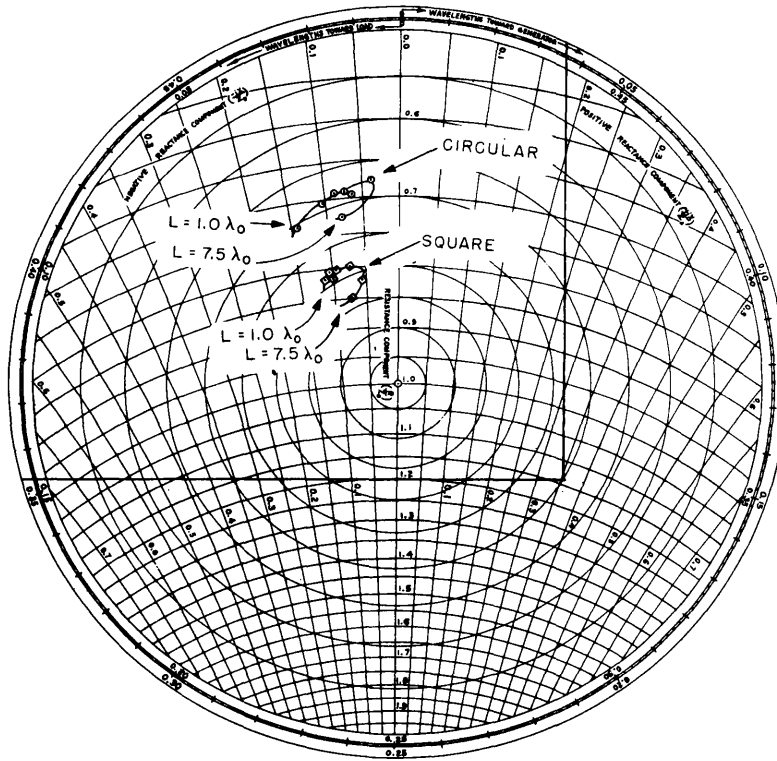


Figure 41 - Polyrod input impedance, measured at the RG-52/U waveguide flange, 9375 Mc, circular and square apertures

A single impedance-matching device in either feed will effectively match all rods of the aperture criterion providing the aperture and taper are similar to the uniform-taper rods. The square-section rod (vswr = 1.20) is somewhat better matched than the circular (vswr = 1.39). Wrapping the rod-feed junctions of these rods with properly dimensioned Fiberglas reduces the mismatch (vswr = 1.15).

Power Capacity

The power capacity of polyrod antennas is limited by voltage breakdown in the feed. The standard waveguide should break down before the square feed, providing the dielectric sections and the charged surfaces are in intimate contact with the current-conducting surfaces. The circular feed has a lower breakdown than the square form, since a portion of the charged dielectric is slightly separated from the current-carrying walls of the waveguide taper section. Both feeds were found to transmit at least 50 kilowatts peak power or 40 watts average at X-band frequencies.

Bandwidth

Since the phase velocity of directive dielectric rods changes fairly rapidly with frequency, these antennas are somewhat frequency sensitive. No attempt was made to measure the full bandwidth as it is more than adequate for most requirements.

Halliday and Kiely (5) claimed ± 20 percent bandwidth on the basis of marked pattern deterioration, sidelobes rising with shorter wavelengths, and beamwidth and back radiation mounting with longer wavelengths. Mallach (9) claimed ± 30 percent on the basis of half-power reduction in gain.

Polarization

The rod antenna will radiate and receive either linear or circular polarization depending on the design of the feed. Linearly polarized antennas designed by the aperture criterion have a cross-polarization sensitivity of approximately minus 28 db; a circularly polarized antenna of uniform-taper form was designed with the results shown in Table 5. The pattern and gain were slightly degraded from the corresponding linear form, mostly due to the unnecessarily large connector flange close to the feed aperture. With the polarizing wedge located at 45 degrees to the E-vector, ± 1.6 db ellipticity was obtained, but the wedge could be relocated to obtain circular polarization or various degrees of ellipticity. With circularly polarized antennas finding wider use in radar, guided missiles, countermeasures, and other applications, the circularly polarized polyrod should be considered for many of these applications.

FUSELAGE PROXIMITY MEASUREMENTS

Microwave antennas of large aperture are known to be sensitive to fuselage reflections, especially under conditions near grazing incidence. Polyrods possess such small apertures that it became desirable to measure the radiation effects caused by nearby reflectors, in order to establish whether the additional physical clearance

TABLE 5
Linearly and Circularly Polarized Antennas, $L = 4\lambda$

Polarization	Gain (db)	Beamwidth (deg)	Sidelobe Depth (db)
Circular	11.5 ± 1.6	34	-12
Linear	15.4	31	-13

could be utilized. This would reduce the aerodynamic loading of externally mounted polyrods, which must scan in various directions during radar searching and tracking operations.

Fixed dielectric rods, or rods which are to be scanned only in one plane, may be constructed of half aperture (10) under the image principle, so that the mounting distance (spacing between the rotation plane and the fuselage) is zero. Such a scanner requires the use of a rotating fuselage section or plate.

In the more general case, full hemispherical scanning, it will be shown that the appreciable beamwidth and sidelobes of single directive rods necessitate a large separation of the rod and fuselage when the fuselage is large. Smaller angular scanning ranges (less than ± 90 degrees normal to the fuselage) allow the use of a shorter mounting distance; conversely, larger mounting distances allow the use of larger scanning ranges.

The impedance, radiation pattern, and gain effects were measured for a few pertinent cases at 9375 Mc. Most of the data were obtained using the APG-18 (XN-1) experimental polyrod. This rod was considered fairly good at the time, but has high sidelobes compared to the newly developed three-taper rod. Parameters investigated include mounting distance, antenna angle, polarization, fuselage span, fuselage material, and form of antenna.

It is noted that rod arrays can undoubtedly be used to reduce the indicated proximity limits of single rods, because of their narrower beams and lower sidelobes.

Standing-Wave Ratio

For this test, the APG-18 rod antenna was mounted close to a flat metal reflector, 11 by $7\lambda_0$ in extent, with various configurations of mounting distance, alignment angle, and polarization. Figure 42 applies to parallel alignment of the rod and reflector, with the reflector in either plane of polarization. The reflector effect is not detected for values of mounting distance D greater than $1.4\lambda_0$ when the polyrod parallels the fuselage, and decreases as the antenna angle increases. The effect is much smaller for parallel incidence polarization (fuselage in the E-plane) than for the other orthogonal polarization. It will become evident that radiation deterioration determines the proximity limitation, rather than the impedance effects.

Proximity Limitation

The proximity limitation may be defined in terms of the useful angular scanning range for which fuselage effects are not objectionable, i.e., $\pm (90 - \phi_m)$, where ϕ_m is the maximum antenna angle for which the fuselage effects are negligible (for any particular system or equipment). Thus, if the fuselage effects, as indicated by the patterns and tracking records, are negligible for $\phi_A \geq 40$ degrees (for a certain application of specified mounting distance, and fuselage span) then the useful scanning range is ± 50 degrees from normal to the fuselage.

Pattern Tests

Radiation patterns were obtained by rotating the polyrod and the fuselage together in a horizontal plane, the polyrod and fuselage maintaining a constant relative spacing and relative alignment (Figure 43). That is, D and ϕ_A remain constant during each pattern, while the detected one-way power is recorded versus ϕ_T . The transmitter illumination proceeds

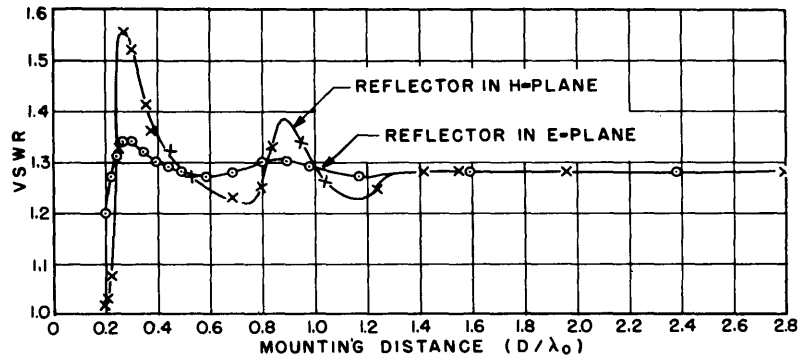


Figure 42 - Influence of mounting distance upon voltage-standing-wave-ratio, for a $7.5\lambda_0$ polyrod parallel to a flat metal fuselage

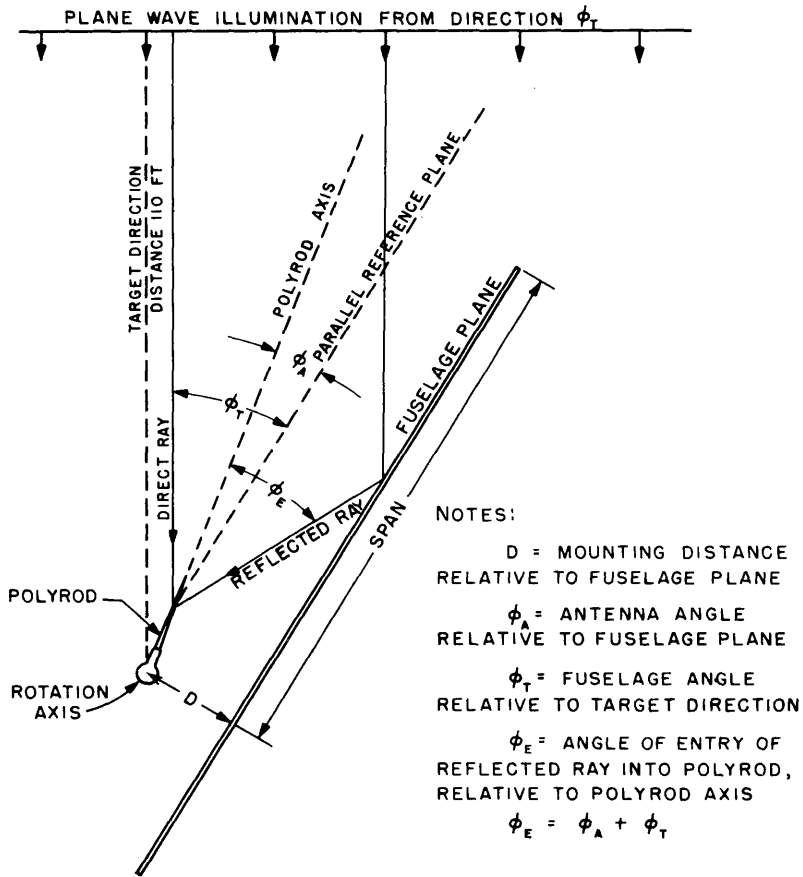


Figure 43 - Diagram for radiation tests

from the direction ϕ_T , some of the rays impinging directly upon the polyrod, and others by reflection from the fuselage. Analogously, ϕ_T may be regarded as the radar target angle by substituting a target for the transmitting antenna and considering the target as moving around the airborne polyrod. Power is given for one-way transmission, as measured.

The large reflector, which simulates the flat fuselage of a large aircraft, is 8 feet long and 20 inches high, and extends 7 feet from the axis of rotation, a span of $64\lambda_0$ at 9375 Mc. The polyrod extends $12.9\lambda_0$ from the same axis. Absorbing material which was designed to reduce the reflections at least 6 db for parallel incidence polarization impinging at any angle between 0 and 84 degrees from the normal, was employed to completely cover the reflector.

Effects of Mounting Distance upon Patterns, $\phi_A = 0$

Radiation patterns obtained with the $64\lambda_0$ (span) fuselage parallel to the polyrod ($\phi_A = 0$), for rotation in the H-plane, are shown in Figure 44. Additional maxima and minima are created in the main and minor lobes of the free-space polyrod patterns for positive angle ϕ_T , the number increasing with mounting distance, and the intensity decreasing. The angle of entry of both the direct and reflected rays into the polyrod, relative to the longitudinal axis of the rod, is ϕ_T degrees, but the rays enter on opposite sides of the rod. The patterns are also affected by the geometric shadow of the fuselage as evidenced by the asymmetry of the patterns. The presence of diffraction at the end of the fuselage results in detection for angles less than that for complete optical shadow, $-\arctan D/51.1\lambda_0$. The radiation deterioration is quite serious over the whole range of mounting distances measured, $D = 4 - 18$ inches ($3.2 - 14.3\lambda_0$ at 9375 Mc). Similar results are available for rotation in the E-plane, which indicate pattern destruction practically as great as for rotation in the H-plane.

Figure 45 shows the influence of absorbing material covering the large reflector upon the H-plane pattern, $D = 12$ inches. Data is available for $D = 3.2$ to $9.5\lambda_0$, showing that some improvement results with the absorber, but the improvement will be more apparent in the tracking records. The effects of absorbing material designed for perpendicular incidence polarization (rotation in the E-plane) were not measured, but should show similar slight improvement.

Smaller flat metal reflectors were tested, which show much less pattern deterioration than the large span. Figure 46 compares the effects of fuselage span upon the E-plane patterns, for $D = 6.3\lambda_0$ and the polyrod parallel to each fuselage ($\phi_A = 0$). The main beam is relatively unaffected for spans shorter than about $13\lambda_0$, but the sidelobes are much more sensitive, and increase with the span length.

The influence of mounting distance with the smaller reflector is indicated in Figure 47, E-plane patterns. A 4.5 db sidelobe appears 19 degrees off axis for the case of $D = 3.2\lambda_0$ (not shown) and the beam is sharpened. The main beam is relatively undisturbed for $D \geq 6.3\lambda_0$ but a 10 db sidelobe appears at $\phi_T = 32$ degrees. Thus the sidelobes lower continuously at least out to $D = 9.6\lambda_0$.

The pattern destruction of the polyrod is no worse than that which is suffered by other antennas of similar free-space characteristics. A rectangular metal horn with a practically triangular main beam and negligible sidelobes showed the same fuselage effects as the polyrod.

Effects of Antenna Angle upon Patterns, $D = 6.3\lambda_0$

Patterns were obtained with the large reflector at several angles relative to the polyrod, $\phi_A = 0, 15, 30, 60,$ and 90 degrees, with $D = 6.3\lambda_0$ (Figure 48). The results for rotation in the

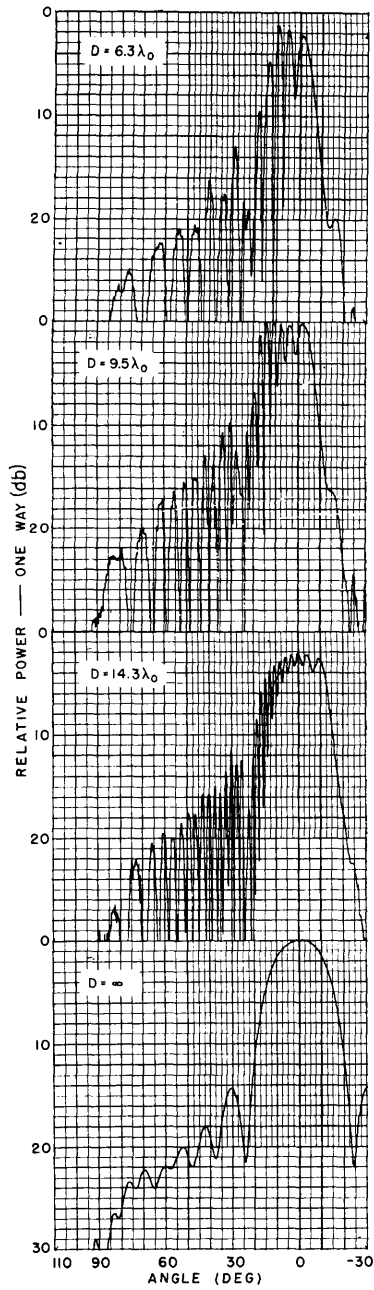


Figure 44 - Patterns showing influence of mounting distance for $\phi_A = 0$, rotation in H-plane

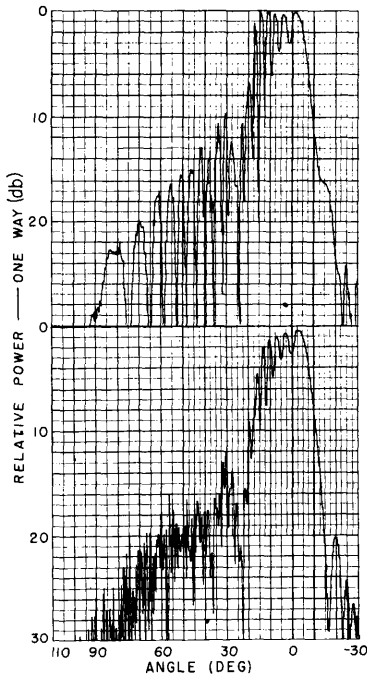


Figure 45 - Patterns showing influence of absorbent X-band fuselage material designed for this polarization. Top - without absorbent material; Bottom - with absorbent material (parallel incidence, rotation in H-plane, $D = 9.5\lambda_0$)

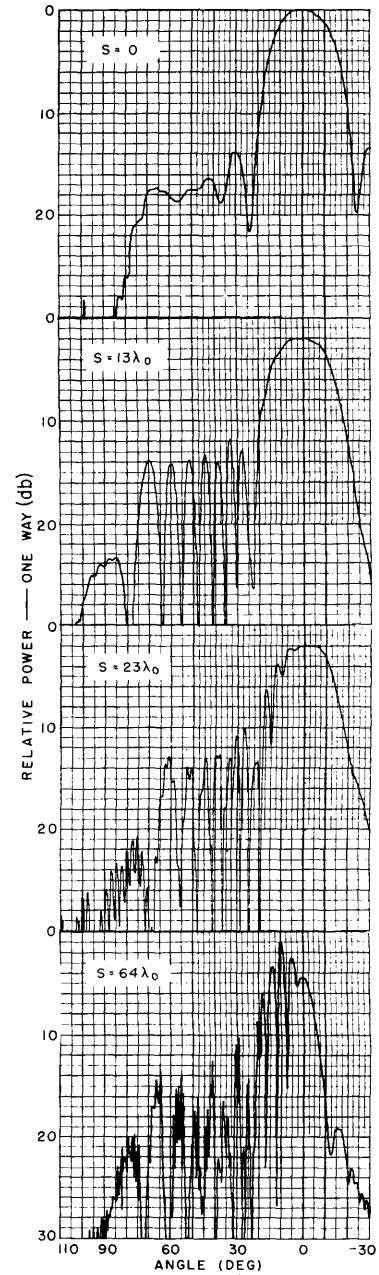
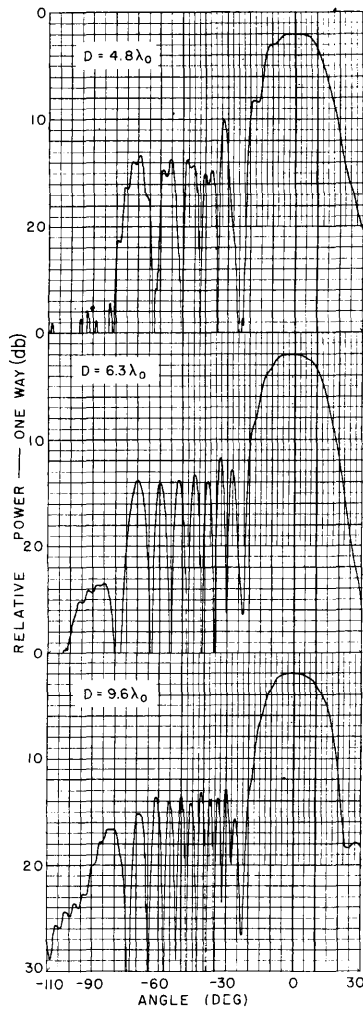


Figure 46 - Patterns showing influence of fuselage span, $D = 6.3\lambda_0$, rotation in E-plane



← Figure 47 - Patterns showing influence of mounting distance using a fuselage of span $13\lambda_0$, rotation in E-plane

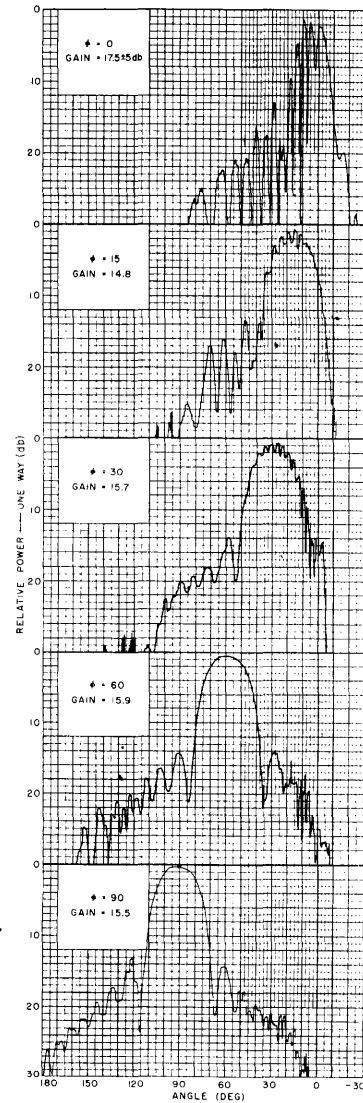


Figure 48 - Patterns showing influence of ground plane for various angles of tilt (ϕ) between antenna and ground plane, for $D = 6.3\lambda_0$, rotation in H-plane →

two principal planes of polarization are much alike, and only the H-plane patterns are shown. The pattern destruction is serious over most of the range of antenna angle. Destruction is quite marked in the main beam for ϕ_A much less than 60 degrees, and is perceived in the sidelobes even with the antenna pointing directly away from the fuselage ($\phi_A = 90^\circ$). The latter patterns ($\phi_A = 90^\circ$) are very similar to the free-space patterns, due to the low backlobes of the polyrod. The fuselage effect will decrease, of course, for greater mounting distances over the range of ϕ_A . The effects of absorbent material and smaller reflector spans were measured only for $\phi_A = 0$, but the qualitative results are obvious and quantitative data can be approximated for other antenna angles.

Tracking Tests

Tracking records were obtained by rotating only the fuselage, maintaining the polyrod pointed directly at the transmitting antenna (Figure 43). The antenna angle, ϕ_A , equals the

target angle, ϕ_T , during each record, D is constant, and the detected one-way power is recorded versus ϕ_T .

These records simulate on-target tracking where the bearing angle of the target is ϕ_T from the fuselage. The data are suitable for the study of gun-laying and other radar tracking operations. Perfect tracking of a perfect radar target is assumed, and the effect of varying phase addition of the direct and reflected waves produce an apparent variation or fluctuation of the main beam gain. The tracking records are, therefore, plots of the variation of main beam gain versus target angle relative to the fuselage.

Tracking Records

Figure 49 shows tracking records for tracking (rotation) in the H-plane of polarization, with the polyrod mounted various distances from the large reflector, where $\phi_T = 90^\circ$ corresponds to the antenna pointing away from the fuselage, and $\phi_T = 0^\circ$ corresponds to parallel alignment and grazing incidence. A straight horizontal trace would represent constant antenna gain throughout the scanning range.

The records indicate that the gain fluctuations decrease with increasing D and ϕ_A , in conformity with the radiation pattern data. For tracking in the H-plane, the fluctuation is not detected at any mounting distance, 3.2 - 14.3 λ_0 , throughout a scanning range of ± 50 degrees ($\phi_A > 40^\circ$). However, the E-plane data is not so favorable.

According to the theory of microwave reflection from a flat conductor, the reflection coefficients of the metals are practically unity and independent of the incidence angle for any polarization. Thus any differences between the H- and E-plane data must be due to differences in the H- and E-plane free-space patterns of the polyrod used. It is apparent that the gain fluctuations of the E-plane data (Figure 50), which extend out to ϕ_A almost 90 degrees, are due to the higher sidelobes in the E-plane of the rod. The sidelobe energy above the -20 db level, in the free-space patterns, extends to only 45 degrees off axis in the H-plane, but out to 80 degrees in the E-plane. The sidelobe reduction methods employed in the present study were not especially effective in this region, and it was not expected that the minor difference of the two polarization patterns would be very important.

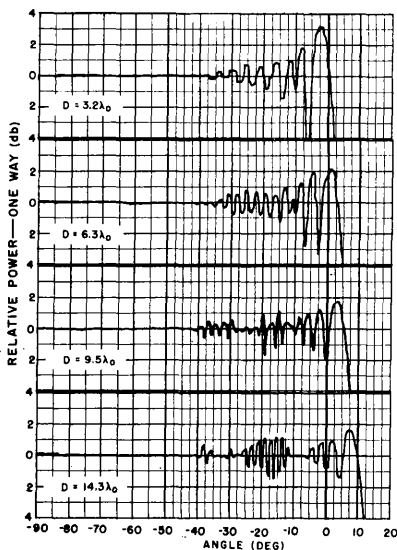


Figure 49 - Tracking records showing influence of mounting distance for antenna on-target, rotation in H-plane

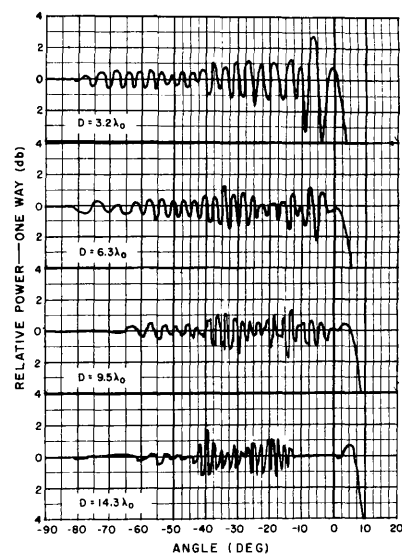


Figure 50 - Tracking records showing influence of mounting distance for antenna on-target, rotation in E-plane

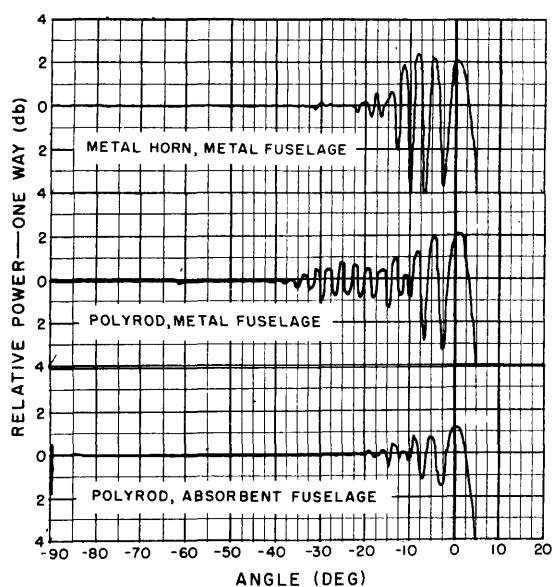


Figure 51 - Tracking records showing influence of antenna type and fuselage material, $D = 6.3\lambda_0$, rotation in H-plane

For tracking in the E-plane, fluctuations extend out to 82 degrees even for a mounting distance of $14.3\lambda_0$, so that the zero-fluctuation scanning range is too small for any use.

The gain fluctuation of a shorter polyrod, (not shown) as well as the metal horn previously mentioned (Figure 51) were just as great as those of the $7.5\lambda_0$ rod. Due to the absence of sidelobes for the horn, however (below -35 db), the gain fluctuations for $D = 6.3\lambda_0$ extend out only to $\phi_A = 32$ degrees.

Covering the large reflector with absorbent material designed for parallel incidence polarization yields marked improvement for rotation in the H-plane (Figure 51). For $D = 6.3\lambda_0$, the scanning range for zero gain fluctuation is broadened from ± 50 degrees to ± 70 degrees.

Measurements were not made of the effects of absorbing material designed for scanning in the E-plane, or of the effects of gain fluctuation with smaller metal reflectors.

CONCLUSIONS

Dielectric-guide antennas effect considerable size, weight, streamlining, and strength improvements over conventional antennas, for applications where their limited characteristics suffice.

Single tapered-rod and tube antennas are suitable for radar, guided missile, counter-measures, and other applications where extremely sharp beamwidths are not required. Long rods provide sharper beamwidth than tubes, and are more suitable for arrays; short thick-walled tubes possess advantages comparable to those of short rods, yielding sharper beamwidth and higher minor lobes.

Rod arrays may be used for great directivity and very sharp beams. To reduce the required driving torque for scanning, they may be mounted upon high-speed aircraft by means of small slotted rotating turrets which shield only the feeds. Dielectric rods cannot be mounted closer to aircraft fuselages than other antennas of similar free-space radiation, even though they are of very small aperture.

It is concluded that there are inherent limitations in single dielectric-guide antennas which cannot be overcome. Thus, sidelobes of highly directive single rods have never been suppressed greater than about 20 db below the main beam. Beamwidth has never been sharpened to less than 21 degrees for reasonable sidelobe suppression, and gains have been limited to 17.6 ± 0.7 db.

RECOMMENDATIONS

Dielectric-guide antennas are recommended for airborne radar and beacon application, particularly at S- and X-bands where they are compact and light. They afford axial or broadside

directivity, and the radiation will suffice for many purposes. Uniform- and multiple-tapered rods are recommended as affording better over-all performance than other forms of dielectric guides. Design may be facilitated by use of the incorporated generalized information. The polyrod should be considered for wider application in radar, guided missiles, counter-measures, etc., where linear or circular polarization is desired. Further modeling tests are recommended for dielectric tubes and discs, and further development of low-constant dielectrics, strengthening methods, and means of pattern control are recommended for end-fire dielectric rods.

* * *

REFERENCES

- (1) Carson, J. R., Mead, S. P., and Schelkunoff, S. A., "Hyper-Frequency Waveguides—Mathematical Theory," Bell System Tech. J. 15: 310-333, 1936
- (2) Dillon, R. E., and Eyges, L. J., "Compact Horns Intermediate Between Polyrods and Reflectors," Rad. Lab., M.I.T., Report No. 961 (Unclassified), 1946
- (3) Eaton, J. E., "Dielectric Rod End-Fire Antennas Close to Metal Surfaces," Rad. Lab., M.I.T., Report No. 969 (Restricted), 1946
- (4) Friis, H. T., and Lewis, W. D., "Radar Antennas," Bell System Tech. J. 26: 278-282, 300-303, 1947
- (5) Halliday, D. F., and Kiely, D. G., "Dielectric-Rod Aerials," I.E.E. J.94, Part III A: 610-618, 1947
- (6) Hondros, D., and Debye, P., "Elektromagnetische Wellen an Dielektrischen Drähten," Ann.Phys. 32: 465-476, 1910
- (7) Lindner, W. J., "The Dielectric Rod Antenna," Tech. Intel. Div., AMC, F-TR-1181-ND, 1949
- (8) Lindsey, W. F., "Drag of Cylinders of Simple Shapes," NACA Report No. 619, 1938
- (9) MacFarlane, G. G., S/Ldr., "Report on Interrogation of Dr. Mallach, V.I.F.S.," C.I.O.S. Evaluation Report No. 273 (Restricted), 1945
- (10) Mallach, P., "Dielectric Beam Antennas for DM and CM Waves," from "Ausgewählte Fragen über Theorie und Technik von Antennen, Part 2," Naval Research Laboratory Translation No. 50 (Unclassified)
- (11) Mueller, G. E., "The Dielectric Antenna or Polyrod," Bell Tele. Lab. Memo., 1942
- (12) Mueller, G. E., "Dielectric Antennas, First Quarterly Progress Report," Ohio State University Report 354-1 (Unclassified), 1949
- (13) Mueller, G. E., and Tyrrell, W. A., "Polyrod Antennas," Bell System Tech. J. 26: 837-851, 1947
- (14) Southworth, G. C., "Hyper-Frequency Waveguides—General Considerations and Experimental Results," Bell System Tech. J. 15: 284-309, 1936
- (15) Southworth, G. C., "Some Fundamental Experiments with Waveguides," Proc. I.R.E. 15: 807-822, 1937
- (16) Stingley, V. G., LTJG, USNR, "Comm. and Radar Polyrod Antennae in Germany," ComNavEu Report, Serial X-2038 (Restricted), 1945

- (17) Von Hippel, A., "Tables of Dielectric Materials," Vols. I, II, III, Laboratory for Insul. Research, M.I.T. (Unclassified), 1944, 1945, 1948
- (18) Watson, R. B., and Horton, C. W., "The Radiation Patterns of Dielectric Rods—Experiment and Theory," J. Applied Phys. 19: 661-670, 1948
- (19) Wegener, "The Speed of Propagation, the Wave Resistance and Damping of Electromagnetic Waves at Dielectric Cylinders," ZWB Report, 1941. Translated by M.O.S., London. M.O.S. Report No. GDC 10/1498T (Unclassified), 1949
- (20) Whitmer, R. M., "Waveguides without Metal Walls," Rad. Lab., M.I.T., Report No. 726 (Unclassified), 1945. Abstracted in Electronics, p. 222, October 1946
- (21) Wilkes, G., "Wavelength Lenses," Proc. I.R.E. 36: 206-212, 1948
- (22) David Taylor Model Basin ltr F2T-B-37 (650: RTP; clb) to BuAer, dated 23 March 1951
- (23) BuShips Specifications RE 13A825C, 4 May 1944

* * *

APPENDIX Measurement Techniques

Standard techniques were used to obtain the E- and H-plane radiation patterns. Field equipment included an M.I.T. Mod 12 modulator, 2J51 magnetron, twelve-inch paraboloid, test antennas, Sperry Type 821 bolometer in a waveguide or coaxial detector mount, and a modified M.I.T. Mark 3 Automatic Pattern Recorder.

The transmission path was 110 feet long and 24 feet above roof level, ensuring negligible sensitivity to roof reflection. The illumination across the test area was substantially a plane wave, since the phase varied less than $\lambda_0/16$, and the intensity varied less than 0.4 db.

Recorded noise level was lower than the power received by an antenna of -17 db absolute gain, allowing pattern resolution throughout a 34 db power range for the most directive antennas tested. Recorder error was less than 0.1 db throughout this range, for the most recent measurements—earlier patterns have been recalibrated and the corrected power scale attached. Absolute gain was measured by comparison of signals received by the test antennas and a horn standard calibrated within 0.3 db error, resulting in absolute gain data accurate to within 0.7 db maximum error. Recorded sidelobe depths and angular coordinates are within maximum errors of 0.4 db and 0.5 degree, respectively.

Antenna dissipation was computed as the decibel sum of the radiator loss (α_r) and feed dissipation (α_f = dielectric and conductor losses). Directivity was obtained by summing gain and dissipation (db), or by planimeter integration of the patterns.

Radiator and antenna input impedances were measured using conventional slotted sections and specially constructed dummy loads. Vibration tests were conducted in three planes on platforms oscillating at 10-55 cps with amplitudes of ± 0.06 in., in accordance with BuShips Specifications RE 13A825C, dated 4 May 1944.

* * *